XDH-1 inactivation causes xanthine stone formation in *C. elegans* which is inhibited by SULP-4-mediated anion exchange in the excretory cell

Jennifer Snoozy[1], Sushila Bhattacharya[1], Robin R. Fettig[1,3], Ashley Van Asma, Chloe Brede[1], Kurt Warnhoff[1,2]

[1]Pediatrics and Rare Diseases Group, Sanford Research, Sioux Falls, SD 57104, USA

[2]Department of Pediatrics, Sanford School of Medicine, University of South Dakota, Sioux Falls, SD 57105 USA

[3]Department of Basic Biomedical Sciences, Sanford School of Medicine, University of South Dakota, Vermillion, SD 57069, USA

Correspondence to: Kurt Warnhoff (kurt.warnhoff@sanfordhealth.org)

Abstract:

Xanthine dehydrogenase (XDH-1) is a molybdenum cofactor (Moco) requiring enzyme that catabolizes hypoxanthine into xanthine and xanthine into uric acid, the final steps in purine catabolism. Human patients with mutations in *xdh-1* develop xanthinuria which can lead to xanthine stones in the kidney, recurrent urinary tract infections, and renal failure. Currently there are no therapies for treating human XDH-1 deficiency. Thus, understanding mechanisms that maintain purine homeostasis is an important goal of human health. Here, we used the nematode *C. elegans* to model human XDH-1 deficiency using 2 clinically relevant paradigms, Moco deficiency or loss-of-function mutations in *xdh-1.* Both Moco deficiency and *xdh-1* mutations caused the formation of autofluorescent xanthine stones in *C. elegans*. Surprisingly, only 2% of *xdh-1* null mutant *C. elegans* developed a xanthine stone, suggesting additional pathways may regulate this process. To uncover such pathways, we performed a forward genetic screen for mutations that enhance the penetrance of xanthine stone formation in *xdh-1* null mutant *C. elegans*. We isolated multiple loss-of-function mutations in the gene *sulp-4* which encodes a transmembrane transport protein homologous to human SLC26 anion exchange proteins. We demonstrated that SULP-4 acts cell-nonautonomously in the excretory cell to limit xanthine stone accumulation. Interestingly, *sulp-4* mutant phenotypes were suppressed by mutations in genes that encode for cystathionase (*cth-2)* or cysteine dioxygenase (*cdo-1*), members of the sulfur amino acid metabolism pathway required for production of the osmolyte taurine. Furthermore, *cdo-1* mRNA accumulated in *sulp-4* mutant animals, mirroring *cdo-1* activation observed during hyperosmotic stress in *C. elegans* and mammals. We propose that loss of SULP-4-mediated anion exchange causes osmotic stress and *cdo-1* activation, a maladaptive response that promotes xanthine stone accumulation. Supporting the model that the osmotic stress response impacts xanthine stone accumulation, a mutation in *osm-8* that constitutively activates the osmotic stress response, also promoted xanthine stone accumulation in an *xdh-1* mutant background. Thus, our work establishes a *C. elegans* model for human XDH-1 deficiency and identifies *sulp-4* and the osmotic stress response governed by *cdo-1* as critical players in controlling xanthine stone accumulation.

Background:

Purines are an abundant and fundamental metabolite class that are essential for the generation of RNA and DNA molecules while purine nucleotides are critical energy sources (ATP) and signaling molecules (GTP). Failures in purine metabolism can lead to both common and rare diseases. For instance, oncogenic mutations activate nucleotide biosynthetic capacity in diverse cancers, promoting cancer progression [1]. Mutations in enzymes in the purine metabolic pathway cause rare inborn errors of metabolism such as Lesch-Nyhan syndrome, purine nucleoside phosphorylase deficiency, and xanthinuria [2-5]. Thus, understanding the mechanisms that impact purine homeostasis is an important goal of human health.

Xanthinuria, an inborn error of purine metabolism, is caused by inactivation of xanthine dehydrogenase (XDH), the terminal enzyme in purine catabolism that oxidizes hypoxanthine to xanthine and xanthine to uric acid [6] (**Fig. 1A**). There are two types of human xanthinuria; type I is caused by mutations in the gene encoding the xanthine dehydrogenase enzyme and type II is caused by mutations in enzymes that synthesize the molybdenum cofactor (Moco), an essential prosthetic group for XDH [4, 5]. Both forms of xanthinuria present with high levels of xanthine in the urine and low levels of uric acid which can result in the formation of xanthine stones in kidneys and muscles, sometimes causing renal failure. There is currently no curative therapy for xanthinuria, however high fluid intake and low purine diets are recommended for patients [7].

XDH requires Moco for its enzymatic function. Moco is a prosthetic group that is required for development in animals ranging from the nematode *C. elegans* to humans [4, 8]. Moco is synthesized by an ancient and conserved biosynthetic pathway [9]. *C. elegans* has recently emerged as a powerful model system for studying Moco biology, and the genes that encode the Moco biosynthetic pathway are termed *moc* in *C. elegans* for MOlybdenum Cofactor biosynthesis [8, 10]. In addition to endogenous Moco synthesis, *C. elegans* can also acquire and use Moco from its bacterial diet [8, 11, 12]. Given its genetic tractability and the ability to manipulate animal Moco content by simple dietary manipulation, *C. elegans* is a useful model for understanding the biology of Moco and Moco-requiring enzymes, such as XDH.

Here, we genetically explored the formation of xanthine stones in *C. elegans,* which emerge during Moco deficiency or in *xdh-1* mutant *C. elegans,* mirroring type I and type II human xanthinuria [4, 5]. Surprisingly, only a small percentage of Moco-deficient and *xdh-1* mutant *C. elegans* developed xanthine stones, suggesting additional parallel pathways for maintaining purine homeostasis. To identify novel regulators of xanthine stone accumulation, we performed an unbiased chemical mutagenesis screen for mutations that enhanced the penetrance of xanthine stone formation in *xdh-1* mutant animals. In this screen we recovered five loss-of-function alleles of *sulp-4,* a gene which encodes a member of the sulfate permease family of transporters with homology to human SLC26 transporters [13]. We demonstrated that SULP-4 acts in the *C. elegans* excretory cell, analogous to the human kidney, to inhibit the accumulation of xanthine stones [14]. We further showed that *sulp-4* was required for normal development. Interestingly, we found that phenotypes caused by *sulp-4* loss of function were suppressed by inactivating mutations in

cth-2 or *cdo-1,* genes that encode core members of the sulfur amino acid metabolism pathway required for synthesis of the osmolyte taurine [8]. We suggest that *sulp-4* loss of function promotes xanthine stone accumulation because of disrupted osmotic homeostasis. This model is supported by the observation that mutations in *osm-8* that constitutively activate the osmotic stress response, also promote xanthine stone accumulation in an *xdh-1* mutant background. Thus, our work establishes a *C. elegans* model for the rare genetic disease xanthinuria and identifies *sulp-4* as a potent genetic modifier of this disease pathology in *C. elegans,* likely acting through disrupted osmotic homeostasis.

Results:

XDH-1 inactivation caused the accumulation of xanthine stones in *C. elegans*.

To explore the pathology of Moco deficiency in the nematode *C. elegans,* we cultured *cth-2; moc-1* and *moc-1 cdo-1* double mutant animals on wild type (Moco replete) or *ΔmoaA* mutant (Moco deficient) *E. coli*. The *moc-1* mutation prevents the endogenous synthesis of Moco while the *cth-2* and *cdo-1* mutations suppress the lethality typically associated with animal Moco deficiency [8]. Thus, by changing the dietary *E. coli*, we can control whether the animals have Moco. When culturing *cth-2; moc-1* double mutant animals on Moco- *E. coli* we surprisingly observed animals that developed autofluorescent stones, typically found in the posterior of the intestine. 54% of *cth-2; moc-1* animals fed a Moco- diet developed an autofluorescent stone while 0% of *cth-2; moc-1* animals developed an autofluorescent stone when fed a diet that provided Moco. We observed similar results for *moc-1 cdo-1* double mutant animals where 17% of animals developed an autofluorescent stone on Moco- *E. coli* and 0% developed a stone when fed wild-type *E. coli* (**Fig. 1B**). Thus, we conclude that the formation of these autofluorescent stones is caused by Moco deficiency.

Surprisingly, we also observed the formation of autofluorescent stones in 8% of wild-type *C. elegans* when cultured on Moco- *E. coli.* 0% of wild-type animals developed an autofluorescent stone when fed Moco+ *E. coli* (**Fig. 1B**). This result demonstrates that dietary Moco deficiency alone is sufficient to promote the formation of autofluorescent stones. This result is surprising as wild-type animals are still competent to produce Moco through their endogenous biosynthetic pathway. However, these data are consistent with our recent findings that the *C. elegans* diet plays a significant role in promoting Moco homeostasis [12].

Given that the development of these autofluorescent stones was dependent upon dietary Moco deficiency, we reasoned that the phenotype was likely being caused by inactivation of one of the four animal Moco-requiring enzymes. Interestingly, inactivation of the Moco-requiring enzyme xanthine dehydrogenase causes the accumulation of insoluble and fluorescent xanthine stones in organisms as diverse as plants, fruit flies, and humans [5, 15-19]. We therefore hypothesized that the autofluorescent stones we observed during *C. elegans* Moco deficiency were xanthine stones. To test this, we looked for the presence of autofluorescent stones in animals carrying the *ok3234* null mutation in *xdh-1,* the *C. elegans* orthologue of xanthine dehydrogenase. When we cultured *xdh-1* null mutant *C. elegans* on wild-

type *E. coli* we indeed observed the formation of highly autofluorescent stones in 2% of animals (**Fig. 1B,C**). Thus, *xdh-1* was necessary for inhibiting the formation of autofluorescent stones. Consistent with their presence in diverse models of XDH-1-deficiency, we propose that the autofluorescent stones we observe during Moco- and XDH-1- deficiency in *C. elegans* are xanthine stones.

***sulp-4* inhibited the formation of xanthine stones.**

XDH-1 functions at the end of the purine catabolism pathway to oxidize hypoxanthine to xanthine and xanthine to uric acid (**Fig. 1A**). Given the critical position of XDH-1 in purine metabolism, we were surprised that only 2% of *xdh-1* null mutant animals developed a xanthine stone. This result suggests the existence of parallel pathways for maintaining purine homeostasis. To identify additional regulators of purine metabolism, we performed an unbiased chemical mutagenesis screen for mutations that enhanced the penetrance of the xanthine stone phenotype. We mutagenized *xdh-1* mutant *C. elegans* with ethyl methanesulfonate (EMS) and cultured the newly mutagenized animals for 2 generations allowing newly induced mutations to become homozygous [20]. We then cloned single mutagenized F2 animals onto their own petri dish and screened for clones where we observed a high fraction of F3 progeny developing xanthine stones.

Here we describe five new EMS-induced recessive loss-of-function mutations that caused a high penetrance of xanthine stone formation in an *xdh-1* mutant background, *rae299, rae302, rae319, rae320* and *rae326* (**see Methods**). These mutant alleles were prioritized because they displayed strong enhancement of xanthine stone formation and formed a complementation group, indicating they affect a single gene (**see Methods**). To identify the causative genetic lesions in these new mutant strains, genomic DNA from all five strains was analyzed via whole genome sequencing. Our complementation studies suggested that the mutant strains should have novel mutations in a common gene. Only one gene, *sulp-4,* was uniquely mutated in all five strains, strongly suggesting these mutations were causative for the enhanced penetrance of xanthine stone formation in the *xdh-1* mutant animals (**Fig. 2A,B, Table S1**). Among the newly isolated *sulp-4* alleles we found 3 missense and 2 splice site mutations. Based on their recessive nature and molecular identities, we propose that these are loss-of-function alleles of *sulp-4.*

To test the hypothesis that loss of *sulp-4* function causes enhanced xanthine stone accumulation in an *xdh-1* mutant, we used CRISPR/Cas9 to engineer a new *sulp-4* deletion allele, *rae334* [21, 22]. The *sulp-4(rae334)* allele is a 683 bp deletion that eliminates part of exon 1, all of exons 2 and 3, and part of exon 4 (**Fig. 2A**). Thus, we propose that *sulp-4(rae334)* encodes a null allele. The *sulp-4(rae334)* allele strongly enhanced the penetrance of xanthine stone formation in *xdh-1* mutant *C. elegans,* phenocopying the *sulp-4* alleles isolated in our EMS screen (**Fig. 2B**). These data demonstrate that the *sulp-4* lesions identified by whole genome sequencing cause xanthine stone accumulation in *xdh-1* mutant animals. Furthermore, these data show that *sulp-4* acts in parallel with *xdh-1* to inhibit the accumulation of xanthine stones.

The xanthine stones observed in *xdh-1; sulp-4* double mutant animals localized to the posterior of the *C. elegans* intestinal lumen, consistent with the localization of the stones observed in *xdh-1* mutant

animals (**Fig. 2C**). In addition to observing xanthine stones at a higher frequency in *xdh-1; sulp-4* mutant animals, the xanthine stones were also much larger suggesting that *sulp-4* loss of function enhances both the penetrance and expressivity of the xanthine stone phenotype in *xdh-1* mutant animals (**Fig. S1**).

We originally observed the formation of xanthine stones during conditions of Moco deficiency; *cth-2; moc-1* double mutant animals feeding on Moco- *E. coli.* We hypothesized that the *sulp-4* mutation would also enhance the formation of xanthine stones caused by Moco deficiency. To test this, we assayed xanthine stone formation in *sulp-4* single mutant animals cultured on wild-type or Moco- *E. coli*. 89% of *sulp-4* mutant animals developed xanthine stones during dietary Moco deficiency compared to 1% of *sulp-4* mutant animals fed a Moco replete diet (**Fig. S2A**). These data are consistent with our conclusion that *sulp-4* functions to limit the accumulation of xanthine stones caused by XDH-1 inactivation resulting from either Moco insufficiency or an *xdh-1* mutation.

***sulp-4* promoted healthy larval and embryonic development.**

While culturing the *sulp-4(rae334)* mutant strain, we observed that mutant animals were sick and slow growing. Thus, we explored the role of *sulp-4* in development and embryonic viability. To test the impact of *sulp-4* loss of function on developmental rate, we synchronized wild-type, *sulp-4(rae319),* and *sulp-4(rae334)* animals at the first stage of larval development and assayed their growth after 72 hours. We found that *sulp-4(rae334)* animals displayed a severe developmental delay compared to the wild type (**Fig. 2D**). Interestingly, *sulp-4(rae319)* animals showed a more subtle developmental delay. Thus, we propose that *sulp-4(rae334)* is a null allele while *sulp-4(rae319)* represents a hypomorph. Similarly, we observed that *sulp-4(rae334)* caused 18% embryonic lethality while *sulp-4(rae319)* caused 5% embryonic lethality. No embryonic lethality was observed for wild-type *C. elegans* (**Fig. 2E**). Thus, we conclude that *rae334* and *rae319* represent an allelic series for *sulp-4* and that *sulp-4* is necessary for promoting embryonic and larval development in *C. elegans.*

***pnp-1* was necessary for the formation of xanthine stones in *xdh-1; sulp-4* mutants but dispensable for the developmental delay caused by *sulp-4* loss of function.**

To further test the model that the autofluorescent stones observed in *xdh-1; sulp-4* mutant animals were composed of xanthine, we performed genetic epistasis with a null mutation in purine nucleoside phosphorylase (*pnp-1*), a gene necessary for the formation of hypoxanthine and xanthine (**Fig. 1A**) [23]. As previously observed, *xdh-1; sulp-4* double mutant animals displayed 98% autofluorescent stone formation while *pnp-1 xdh-1; sulp-4* triple mutant *C. elegans* displayed 3% formation of autofluorescent stones (**Fig. 3A**). Thus, *pnp-1* was necessary for the formation of the autofluorescent stones observed in *xdh-1; sulp-4* double mutants. Given that *pnp-1* plays a conserved role in the formation of hypoxanthine and xanthine, these results support our model that the autofluorescent stones we observe are likely to be predominantly composed of xanthine. Although, we cannot exclude the possibility that other metabolites, such as hypoxanthine, are also present in the autofluorescent stones.

To determine if *pnp-1* acts in a genetic pathway with *sulp-4,* we tested the impact of *pnp-1* loss of function on the developmental delay displayed by *sulp-4* mutant animals. *pnp-1; sulp-4* double mutant

186 larvae developed at a rate similar to *sulp-4* single mutant animals. Importantly, *pnp-1* mutant animals
187 displayed healthy larval development (**Fig. 3B**). Thus, *pnp-1* was not required for the developmental delay
188 displayed by *sulp-4* mutant *C. elegans.* We propose a genetic pathway where *pnp-1* promotes the
189 formation of xanthine stones epistatic to the function of *xdh-1* and in parallel to the activity of *sulp-4*.
190 ***sulp*-4/SLC26 encodes an anion exchange protein that acted in the excretory cell to promote**
191 **xanthine homeostasis.**
192 *sulp-4* encodes a transmembrane transporter with homology to the SLC26 family of anion
193 transporters in mammals [13, 24]. The *C. elegans* genome encodes eight members of the SLC26
194 transporter family, named SULP-1 through SULP-8 [13]. We wondered if other members of the SLC26
195 family of transporters also played a role in limiting the formation of xanthine stones. To test this, we
196 cultured viable strains with deletions in *sulp-1, sulp-2, sulp-4, sulp-5, sulp-7,* and *sulp-8* on Moco- *E. coli*
197 and assayed the formation of xanthine stones. Only the strain carrying the *sulp-4* mutation displayed a
198 high penetrance of xanthine stones (79%, **Fig. S2B**). Thus, the enhancement of xanthine stone formation
199 is specific to loss of *sulp-4* and not a general feature of *sulp* inactivation.
200 SULP-4 is expressed in the apical membrane of the *C. elegans* excretory cell, a single cell that
201 plays roles in ionic regulation and waste elimination analogous to the mammalian renal system [13, 14,
202 25]. Studies of SULP-4 expressed in *Xenopus* oocytes demonstrate that SULP-4 is sufficient to promote
203 the transport of sulfate and, to a lesser extent, chloride [13]. To determine the site of action of *sulp-4* with
204 respect to the xanthine stone formation phenotype, we generated transgenic *xdh-1; sulp-4* double mutant
205 *C. elegans* expressing a *Psulp-4::SULP-4::GFP* translational fusion transgene (plasmid was a gift from Dr.
206 Keith Nerhke) [13]. Consistent with previous reports, we exclusively saw expression of the *Psulp-4::SULP-*
207 *4::GFP* translational fusion in the excretory cell (**Fig. 4A,B**). To test the functionality of the *Psulp-4::SULP-*
208 *4::GFP* transgene, we performed rescue experiments by generating *xdh-1; sulp-4* double mutant animals
209 expressing *Psulp-4::SULP-4::GFP* and assaying the formation of xanthine stones. *xdh-1; sulp-4* double
210 mutant animals expressing the *Psulp-4::SULP-4::GFP* did not develop xanthine stones, demonstrating
211 functional transgenic rescue. This rescue was observed in three independently derived transgenic strains
212 (**Fig. 4C**). Thus, the *Psulp-4::SULP-4::GFP* transgenic fusion protein was functional, suggesting that its
213 expression pattern faithfully represents endogenous SULP-4 localization. We conclude that SULP-4 acts
214 in the excretory cell to negatively regulate the formation of xanthine stones. Our observation that *xdh-1;*
215 *sulp-4* double mutant animals typically develop xanthine stones in the intestinal lumen suggests that *sulp-*
216 *4* is functioning cell non-autonomously to limit the formation of xanthine stones.
217 To further test the role of the excretory cell in preventing the formation of xanthine stones, we used
218 an *exc-5* mutation that causes defects in excretory cell development and morphology [26]. We reasoned a
219 malformed excretory cell may not function efficiently and thus phenocopy *sulp-4* loss of function with
220 respect to xanthine stone formation. Indeed, *exc-5; xdh-1* double mutant animals displayed enhanced
221 formation of xanthine stones (**Fig. S3A**)**.** Although, the xanthine stone penetrance of the *exc-5; xdh-1*
222 (16%) double mutant strain was modest compared to *xdh-1; sulp-4*. Importantly, *sulp-4* loss of function did

223 not cause defects in excretory cell morphology (**Fig. S3B-D**). We conclude that the enhancement of
224 xanthine stone formation caused by inactivating mutations in *sulp-4* result from loss of SULP-4 anion
225 exchange function and not broader defects in excretory cell biology.

226 ***cth-2* and *cdo-1* were necessary for *sulp-4* mutant phenotypes.**

227 *sulp-4* inactivation caused xanthine stone formation during dietary Moco deficiency (**Fig. S2A, Fig.**
228 **S4A**), demonstrating that the enhancement of xanthine stones caused by *sulp-4* loss of function occurs
229 even when endogenous Moco biosynthesis is functional. To test the impact of a *sulp-4* mutation on
230 xanthine stone formation during complete Moco deficiency, we engineered *sulp-4; cdo-1 moc-1* triple
231 mutant *C. elegans* that cannot synthesize their own Moco (caused by *moc-1* mutation) and are viable
232 during Moco deficiency (caused by *cdo-1* suppressor mutation) (**Fig. 5A**). When cultured on Moco- *E. coli,*
233 *sulp-4; cdo-1 moc-1* triple mutants are completely Moco deficient yet only displayed 9% penetrance of
234 xanthine stones (**Fig. S4A**). Similarly, *sulp-4; cdo-1* double mutant animals cultured on Moco- *E. coli*
235 displayed 0% penetrance of xanthine stones, dramatically reduced compared to the 85% penetrance
236 displayed by *sulp-4* mutants cultured on Moco- *E. coli* (**Fig. S4A**). These results were surprising and
237 suggest that *cdo-1* is necessary for the formation of xanthine stones caused by a *sulp-4* mutation and
238 Moco deficiency.

239 To further test the impact of *cdo-1* on the formation of xanthine stones, we engineered *xdh-1; sulp-*
240 *4; cdo-1* triple mutants. Surprisingly, *xdh-1; sulp-4; cdo-1* triple mutants displayed a 4% xanthine stone
241 penetrance, dramatically reduced when compared to the 98% penetrance displayed by *xdh-1; sulp-4*
242 double mutant animals (**Fig. 5B**). Thus, *cdo-1* was necessary for the formation of xanthine stones
243 displayed by *xdh-1; sulp-4* double mutants. Interestingly, we still observe a low penetrance of xanthine
244 stones in *xdh-1; sulp-4; cdo-1* triple mutants suggesting that *cdo-1* activity is not absolutely required for the
245 formation of xanthine stones but only required for the xanthine stone enhancement caused by *sulp-4* loss
246 of function.

247 *cdo-1* encodes the *C. elegans* cysteine dioxygenase, a critical enzyme in the in sulfur amino acid
248 catabolism pathway that breaks down excess cysteine and methionine and is essential for synthesis of the
249 osmolyte taurine (**Fig. 5A**) [8, 27, 28]. To determine if the impact of *cdo-1* on the enhanced xanthine stone
250 formation caused by *sulp-4* inactivation was a result of impaired sulfur amino acid catabolism, we used a
251 *cth-2* mutation which eliminates the activity of *C. elegans* cystathionase (**Fig. 5A**). Consistent with our
252 results with *cdo-1* loss of function, we found that *cth-2; xdh-1; sulp-4* triple mutant animals also displayed a
253 low 19% penetrance of xanthine stones (**Fig. 5B**). Taken together, these genetic data suggest that sulfur
254 amino acid catabolism is required for the enhancement of xanthine stone accumulation caused by loss of
255 *sulp-4* function.

256 To test whether mutations in *cth-2* or *cdo-1* would suppress the defects in larval and embryonic
257 development displayed by *sulp-4* mutant animals, we assayed larval and embryonic development in *cth-2;*
258 *sulp-4* and *sulp-4; cdo-1* double mutant animals and compared to *sulp-4* single mutant animals. Consistent
259 with their suppression of xanthine stone formation, *cth-2* or *cdo-1* mutations suppressed the

260 developmental delay and embryonic lethality caused by a *sulp-4* mutation (**Fig. 5C,D**). Thus, we conclude
261 that *cth-2* and *cdo-1* are broadly required for phenotypes caused by *sulp-4* loss of function (**Fig. 5E**).
262 **Loss of *osm-8* promoted xanthine stone accumulation in *xdh-1* mutant animals, linking the osmotic**
263 **stress response and xanthine stone formation.**
264 What is the physiological intersection between *sulp-4* and the sulfur amino acid catabolism
265 pathway governed by *cth-2* and *cdo-1*? Given that *sulp-4* encodes an anion exchange protein that
266 functions in the *C. elegans* excretory cell, we hypothesized that *sulp-4* mutant animals may be
267 experiencing osmotic stress even when cultured under normal laboratory growth conditions. To maintain
268 osmotic homeostasis, cellular concentrations of non-ionic osmolytes such as taurine, glycerol, and *myo*-
269 inositol are dramatically increased through activation of osmolyte synthesis or import. This adaptive
270 response normally functions to osmotically equilibrate cells with their environment without dramatically
271 altering ionic composition of the cell.
272 To test the model that *sulp-4* loss of function is causing osmotic stress, we examined the
273 transcription of three genes that are critical for promoting osmolyte accumulation: *cdo-1, gpdh-1,* and *hmit-*
274 *1.1.* As discussed above, *cdo-1* encodes cysteine dioxygenase, an enzyme that is required to produce the
275 osmolyte taurine [28, 29]. *gpdh-1* encodes glycerol 3-phosphate dehydrogenase and is required to
276 produce glycerol, a critical osmolyte [30, 31]. Finally, *hmit-1.1* encodes an H^+/*myo*-inositol transporter and
277 functions to import *myo*-inositol, another important osmolyte [32]. All three of these genes are
278 transcriptionally induced via hyperosmotic stress and by genetic lesions such as *osm-8(n1518)* that
279 activate the hyperosmotic stress response [33]. Using qPCR, we observed that *cdo-1* mRNA was
280 consistently elevated in both *sulp-4* (~8-fold) and *osm-8* (~4-fold) mutant animals compared to the wild
281 type **(Fig. 6A**). Similarly, *gpdh-1* and *hmit-1.1* mRNA also appeared to be mis-regulated in *sulp-4* mutant
282 animals. However, these results showed high variability and were not consistently reproducible when RNA
283 was isolated from either the *sulp-4* or *osm-8* mutant animals (**Fig. S4C,D**). These results were unexpected
284 given the established role of *osm-8* in the transcriptional regulation of *hmit-1.1* and *gpdh-1* [33, 34]. We
285 suspect our rigorous washing of *C. elegans* samples prior to RNA isolation may impact the osmotic
286 environment of our animals, muting the established transcriptional activation of *hmit-1.1* and *gpdh-1* (**see**
287 **Methods)**. Nevertheless, our data demonstrate that *cdo-1* mRNA accumulates during *sulp-4* or *osm-8*
288 inactivation. Thus, we propose that *sulp-4* mutant *C. elegans* may be experiencing hyperosmotic stress.
289 Given that *cdo-1* was necessary for phenotypes caused by *sulp-4* inactivation, we wondered
290 whether inactivating mutations in other osmotic response genes may also suppress *sulp-4* mutant
291 phenotypes. To test this, we engineered *gpdh-1; sulp-4* and *hmit-1.1; sulp-4* double mutant strains of *C.*
292 *elegans* and assayed for the formation of xanthine stones when animals were cultured on a Moco- diet.
293 Unlike *cdo-1,* neither *gpdh-1* nor *hmit-1.1* were necessary for the formation of xanthine stones caused by a
294 *sulp-4* mutation (**Fig. S4B**). These data suggest that the suppression *sulp-4* mutant phenotypes by *cdo-1*
295 loss-of-function is specific and not a general feature of inactivating mutations in genes involved in the
296 osmotic stress response.

297 To determine if activating the hyperosmotic stress response is sufficient to promote xanthine stones
298 in an *xdh-1* mutant background, we used a loss-of-function mutation in *osm-8* that constitutively activates
299 the hyperosmotic stress response in the absence of environmental osmotic stress [33, 34]. Interestingly,
300 *osm-8; xdh-1* double mutant *C. elegans* developed xanthine stones like *xdh-1; sulp-4* double mutant
301 animals (**Fig. 6B)**. Although, the xanthine stones observed in *osm-8; xdh-1* double mutant animals were
302 not as large as those observed in *xdh-1; sulp-4* animals (**Fig. S1).** Furthermore, like *xdh-1; sulp-4* double
303 mutants, *cdo-1* was necessary for the formation of xanthine stones in the *osm-8; xdh-1* double mutant
304 animals, implying a common genetic pathway controlling xanthine stone formation downstream of *osm-8*
305 and *sulp-4* mutations (**Fig. 6B)**. However, it should be noted that *cdo-1* loss of function only partially
306 suppressed the formation xanthine stones in *osm-8; xdh-1* mutant animals. This suggests there may be
307 additional factors downstream of *osm-8* governing xanthine homeostasis. Taken together, these data
308 suggest that proper osmotic regulation is critical to prevent the formation of xanthine stones when *xdh-1*
309 activity is limited.
310
311 **Discussion:**
312 *Modeling xanthinuria in C. elegans.*
313 Human xanthinuria was originally described in 1954, and presents with high urinary xanthine, low
314 uric acid in serum and urine, the formation of xanthine stones, and, in some cases, renal failure [5]. Still,
315 there are no curative treatments for xanthinuria or the formation of xanthine stones. The current
316 recommendation for patients is a high fluid intake and low purine diet [7]. Thus, understanding the cellular
317 mechanisms that regulate the pathology associated with xanthinuria is an important goal.
318 Animal models, such as *C. elegans,* have proven to be powerful tools for exploring the pathology of
319 rare inborn errors of metabolism including NGLY1 deficiency, Moco deficiency, Friedrich's ataxia, and
320 many others [8, 35, 36]. Here we use *C. elegans* to model human type I and type II xanthinuria. We
321 employed genetic strategies to inhibit XDH-1 activity by mutating the *xdh-1* gene (type I) or limiting animal
322 Moco (type II) [4, 5]. Both manipulations recapitulate a critical feature of human XDH deficiency, the
323 formation of insoluble xanthine stones.
324 Interestingly, xanthine stones are highly autofluorescent and visible with a standard fluorescence
325 microscope, a phenotype that has been previously characterized in the model plant *Arabidopsis thaliana*
326 [17]. Given the transparent nature of *C. elegans,* this phenotype empowers genetic analyses of xanthine
327 stone accumulation and, by proxy, purine biology. Here we use the power of *C. elegans* genetics in
328 combination with this simple phenotype to identify and characterize regulators of purine homeostasis.
329 *Defining genetic regulators of xanthine stone formation.*
330 We sought to define genetic regulators of the formation of xanthine stones. Given the established
331 purine catabolism pathway (**Fig. 1A)**, we used a hypothesis-driven approach to define genes that regulate
332 the formation of xanthine stones. Purine nucleoside phosphorylase (PNP-1/PNP) was a lead candidate
333 given its biochemical requirement for the formation of xanthine. Indeed, we demonstrated that *pnp-1* was

334 necessary for the formation of xanthine stones in our *C. elegans* mutant animals. While *pnp-1* loss of
335 function suppressed the formation of xanthine stones in an *xdh-1; sulp-4* double mutant background, it did
336 not suppress the developmental phenotypes caused by *sulp-4* loss of function. These results suggest that
337 *pnp-1* is not acting downstream of *sulp-4* to control development and is consistent with the established
338 role of PNP-1 acting in the purine catabolism pathway with XDH-1 (**Fig. 5E)**. These results suggest that
339 inhibiting the activity of purine nucleoside phosphorylase may be a therapeutic strategy for limiting the
340 accumulation of xanthine and xanthine stones in patients suffering from xanthinuria. However, this
341 treatment strategy may be fraught, given the consequences of PNP inactivation. Human patients with
342 purine nucleoside phosphorylase deficiency display impaired T-cell immunity [3]. In fact, a potent PNP
343 inhibitor has been developed, and induces apoptosis of B- and T-lymphocytes [37, 38]. Thus, the potential
344 benefits of PNP inhibition in the treatment of human xanthinuria patients would need to be evaluated and
345 weighed against the negative impacts on the immune system.
346 To identify new and unexpected regulators of purine homeostasis, we employed an unbiased
347 genetic approach. In a forward genetic screen, we identified *sulp-4* as a potent modifier of xanthine stone
348 formation. Loss-of-function mutations in *sulp-4* dramatically enhanced the penetrance and expressivity of
349 xanthine stone formation in our *C. elegans* model of xanthinuria. These genetic data demonstrate that
350 *sulp-4* normally acts to limit the formation of xanthine stones. Interestingly, we also found that *sulp-4* was
351 necessary for promoting normal larval and embryonic development, as *sulp-4* mutant animals displayed
352 delayed larval development and embryonic hatching defects. *sulp-4* encodes a transmembrane transport
353 protein homologous to human SLC26A5/6 which function in Cl^-/HCO_3 exchange and oxalate secretion in
354 the kidney in addition to secretion of oxalate from the small intestine [39, 40]. Heterologous transport
355 assays of *C. elegans* SULP-4 expressed in *Xenopus* oocyes demonstrate that chloride and sulfate are
356 transported by SULP-4 [13]. Thus, we propose that failures in the transport of these, and potentially other,
357 anions cause the increased xanthine stone accumulation and developmental defects observed in *sulp-4*
358 mutant animals.
359 SULP-4 was previously demonstrated to localize to the apical membrane of the excretory cell,
360 which we also observed [13]. Importantly, we demonstrate that *Psulp-4::SULP-4::GFP* rescues the
361 formation of xanthine stones displayed by an *xdh-1; sulp-4* double mutant animal. This functional rescue is
362 strong evidence that *sulp-4* is acting in the excretory cell to limit the formation of xanthine stones.
363 Interestingly, xanthine stones accumulate in the lumen of the *C. elegans* intestine while *sulp-4* acts in the
364 excretory cell. Thus, we conclude that *sulp-4* acts cell-nonautonomously to limit xanthine stone
365 accumulation. These data establish a new intersection between SULP-4, the excretory cell, and purine
366 homeostasis.
367 *SULP-4 homologues are implicated in calcium oxalate stone formation.*
368 Kidney stones, the formation of solid masses of salts, minerals, or metabolites in the urinary tract,
369 are an important health concern. About 1 out of every 10 individuals in the United States will develop a
370 kidney stone over the course of their lifetimes [41]. Kidney stones are not uniform, and are diverse in

371 composition, frequency, and pathophysiology [42]. For example, calcium oxalate stones account for about
372 half of all reported kidney stones while xanthine stones are exceedingly rare [5].
373 Our genetic studies demonstrate that the SLC26 family member, SULP-4, plays a role in mediating
374 the formation of xanthine stones in *C. elegans.* Interestingly, we are not the first to report a role for SLC26
375 family members in metabolic stone formation. Mouse SLC26A6 has been shown to limit urolithiasis,
376 paralleling our results with *C. elegans* SULP-4. Specifically, SLC26A6 null mutant mice develop a high
377 incidence of calcium oxalate stones in the bladder [43]. Similarly, a dominant negative mutation in
378 SLC26A6 and loss of function mutations in SLC26A1 are proposed to cause calcium oxalate
379 nephrolithiasis in humans [44, 45]. In contrast, the *Drosophila melanogaster* homolog of human
380 SLC26A5/6, dPrestin, promotes the formation of calcium oxalate stones in the Malpighian tubules in a
381 dietarily-induced model of calcium oxalate nephrolithiasis. Under a diet of high oxalate, *Drosophila*
382 develop calcium oxalate stones whose formation is dampened by RNAi knockdown of dPrestin [46]. With
383 respect to calcium oxalate stones, the mechanism of stone formation is believed to relate directly to the
384 role of the SLC26 family members in oxalate transport. Loss of SLC26 proteins results in higher or lower
385 concentrations of oxalate in a given space, altering the likelihood of stone formation. In contrast, we
386 propose that xanthine is the critical component of the stones that form in *xdh-1; sulp-4* mutant animals, not
387 oxalate. In heterologous transport assays, oxalate was not meaningfully transported by SULP-4 [13].
388 However, it is possible that *sulp-4* mutations may enhance the formation of additional metabolic stones
389 given a specific genetic or environmental perturbation. This hypothesis remains to be tested. Regardless,
390 we think it is very intriguing that SLC26 homologues in mouse, humans, flies, and worms have all been
391 shown to play roles in metabolic stone formation and suggests the potential for a fundamental mechanism
392 underlying these discrete observations.
393 *Implications for the osmotic stress response in the formation of xanthine stones.*
394 We next sought to understand the molecular nature of the genetic interaction between *sulp-4* and
395 *xdh-1* with respect to xanthine stone formation. Given that *sulp-4* encodes an anion exchange protein that
396 transports chloride and sulfate ions and acts cell-nonautonomously in the excretory cell, we hypothesized
397 that *sulp-4* mutations may disturb osmotic balance in *C. elegans* [13]. We imagined that disturbed
398 osmoregulation may cause higher solute concentrations in a given fluid (such as the lumen of the *C.*
399 *elegans* intestine) and result in an increased likelihood of stone formation. Disturbances in water
400 homeostasis are known to contribute to stone formation, as dehydration is a key risk factor for human
401 kidney stones [47]. Several lines of evidence support our model that *sulp-4* loss of function is causing
402 disturbed osmotic homeostasis which in turn promotes xanthine stone formation: i) *sulp-4* mutants induced
403 the transcription of *cdo-1,* a gene that is also induced by a high salt diet in both *C. elegans* and mammals
404 [29, 33]. Furthermore, it appears that *sulp-4* loss of function also altered the expression of *gpdh-1* and
405 *hmit-1.1,* additional genes involved in the response to high salt stress [33, 34]. Although, it is important to
406 note that our data supporting this claim are inconsistent and not statistically significant. ii) Activation of the
407 high salt response through a distinct genetic perturbation, *osm-8* loss of function, also promoted the

408 formation of xanthine stones in an *xdh-1* mutant background [34]. iii) Finally, inactivation of CDO-1 which is
409 required for the production of the osmolyte taurine [28], suppressed the enhanced formation of xanthine
410 stones caused by both *osm-8* and *sulp-4* loss of function mutations. Together, these results support the
411 model that, in an *xdh-1* mutant background, activation of the osmotic stress response, and specifically
412 *cdo-1,* is maladaptive and promotes the formation of xanthine stones. While a role for water homeostasis
413 has long been appreciated in the control of kidney stone formation and treatment, our studies uncover a
414 new genetic pathway that regulates these phenomena in a whole animal system and may offer new
415 therapeutic targets for the treatment of urinary stone disease.
416 *Intersection between sulfur amino acid metabolism and Moco-dependent metabolism.*
417 Previous studies in *C. elegans* identified *cth-2* and *cdo-1* loss of function mutations as suppressors
418 of the lethality associated with Moco deficiency and deficiency of the Moco-requiring enzyme sulfite
419 oxidase [8]. Loss of sulfite oxidase is lethal in *C. elegans* and humans due to the accumulation of its
420 reactive and toxic substrate, sulfite [8, 48]. *cth-2* and *cdo-1* inactivation limit the accumulation of sulfites,
421 suppressing the lethality caused by Moco or sulfite oxidase deficiency. Is it a coincidence that loss of *cth-2*
422 or *cdo-1* suppress phenotypes associated with two distinct Moco-requiring enzymes, i) lethality displayed
423 by *suox-1* null mutant animals and ii) xanthine stone formation of *xdh-1; sulp-4* double mutant animals?
424 Given that the substrates and products of these two Moco-dependent enzymes are distinct, it is peculiar
425 that loss-of-function phenotypes of both are modulated by these common genetic factors. Future studies
426 are required to tease apart the potential molecular intersections between CTH-2/CDO-1 and these Moco-
427 dependent pathways.
428 An additional layer of complexity is added when considering the regulation of *cdo-1.* Here, we
429 reinforce previous observations that *cdo-1* is activated in response to hyperosmotic stress [29, 33]. *sulp-4*
430 and *osm-8* mutant *C. elegans* both accumulated *cdo-1* mRNA. Yet, CDO-1/CDO1 levels and activity are
431 also modified by dietary sulfur amino acid content. This regulation includes both transcriptional and post-
432 translational control of cysteine dioxygenase [27, 49-53]. Given that SULP-4 has been shown to mediate
433 sulfate transport and sulfate is a metabolic product of sulfur amino acid metabolism governed by CTH-
434 2/CDO-1/SUOX-1, sulfate seems like a potential metabolic intersection between these seemingly
435 disparate Moco-dependent pathways. Whether there is any overlap between the mechanisms of CDO-
436 1/CDO1 regulation downstream of hyperosmotic stress and high sulfur amino acid content remains to be
437 studied.
438
439 **Materials and methods:**
440 General methods and strains:
441 *C. elegans* were cultured using established protocols [20]. Briefly, animals were cultured at 20°C
442 on nematode growth media (NGM) seeded with wild-type *E. coli* (OP50) unless otherwise noted. The wild-
443 type strain of *C. elegans* was Bristol N2. Additional *E. coli* strains used in this work were BW25113 (Wild
444 type, Moco+) and JW0764-2 (Δ*moaA753::kan,* Moco-) [54].

445 *C. elegans* mutant and transgenic strains used in this work are listed here. When previously
446 published, sources of strains are referenced. Unless a reference is provided, all strains were generated in
447 this study.
448 **Non-transgenic strains:**
449 N2, wild type [20]
450 GR2257, *cth-2(mg599) II* [8]
451 GR2259, *cth-2(mg599) II; moc-1(ok366) X* [8]
452 GR2260, *cdo-1(mg622)* [8]
453 GR2261, *cdo-1(mg622) moc-1(ok366) X* [8]
454 USD869, *xdh-1(ok3234) IV* (Outcrossed 2X)
455 USD1033, *sulp-4(rae319) V* (Outcrossed 4X)
456 USD1037, *sulp-4(rae319) V; cdo-1(mg622) moc-1(ok366) X*
457 USD1038, *sulp-4(rae319) V; cdo-1(mg622) X*
458 USD1055, *xdh-1(ok3234) IV; sulp-4(rae334) V*
459 USD1091, *sulp-4(rae334) V; cdo-1(mg622) X*
460 USD1103, *cth-2(mg599) II; sulp-4(rae334) V*
461 USD1105, *cth-2(mg599) II; xdh-1(ok3234) IV; sulp-4(rae334) V*
462 USD1146, *xdh-1(ok3234) IV; sulp-4(rae334) V; cdo-1(mg622) X*
463 USD1154, *xdh-1(ok3234) IV; cdo-1(mg622) X*
464 USD1163, *pnp-1(jy121) IV* (Outcrossed 1X) [23]
465 USD1170, *cth-2(mg599) II; xdh-1(ok3234) IV*
466 USD1174, *pnp-1(jy121) xdh-1(ok3234) IV*
467 USD1198, *pnp-1(jy121) IV; sulp-4(rae319) V*
468 USD1215, *pnp-1(jy121) xdh-1(ok3234) IV; sulp-4(rae319) V*
469 USD1269, *exc-5(rh232) xdh-1(ok3234) IV*
470 USD1308, *osm-8(n1518) II; xdh-1(ok3234) IV*
471 USD1310, *gpdh-1(ok1558) I* (Outcrossed 4X)
472 USD1312, *hmit-1.1(ok2923) V* (Outcrossed 4X)
473 USD1322, *gpdh-1(ok1558) I; sulp-4(rae319) V*
474 USD1324, *sulp-4(rae319) hmit-1.1(ok2923) V*
475 USD1327, *osm-8(n1518) II; xdh-1(ok3234) IV; cdo-1(mg622) X*
476 NJ731, *exc-5(rh232) IV* [26]
477 MT3571, *osm-8(n1518) II* [34]
478 RB1082, *sulp-5(ok1048) V*
479 RB1366, *sulp-2(ok1551) X*
480 RB1369, *sulp-2(ok1554) X*
481 RB1436, *sulp-1(ok1639) I*

482 RB2134, *sulp-8(ok2842) V*
483 FX08263, *sulp-5(tm8264) X*
484 VC3021, *sulp-7(ok3751) X*
485 VC3045, *sulp-7(ok3752) X*
486 **Transgenic strains:**
487 USD1060, *xdh-1(ok3234) IV; sulp-4(rae319) V; raeEx118*
488 USD1061, *xdh-1(ok3234) IV; sulp-4(rae319) V; raeEx119*
489 USD1062, *xdh-1(ok3234) IV; sulp-4(rae319) V; raeEx120*
490 USD1251, *qpIs11 I; sulp-4(rae319) V*
491 USD1277, *qpIs11 I; exc-5(rh232) IV*
492 BK36, *qpIs11 I; unc-119(ed3) III* [55]
493 **EMS-derived strains:**
494 USD962*, *xdh-1(ok3234) IV; sulp-4(rae299) V*
495 USD1007, *xdh-1(ok3234) IV; sulp-4(rae299) V* (Outcrossed 2X)
496 USD971*, *xdh-1(ok3234) IV; sulp-4(rae302) V*
497 USD997, *xdh-1(ok3234) IV; sulp-4(rae302) V* (Outcrossed 1X)
498 USD990*, *xdh-1(ok3234) IV; sulp-4(rae319) V*
499 USD1001, *xdh-1(ok3234) IV; sulp-4(rae319) V* (Outcrossed 1X)
500 USD1013*, *xdh-1(ok3234) IV; sulp-4(rae320) V*
501 USD1019*, *xdh-1(ok3234) IV; sulp-4(rae326) V*
502 *Whole genome sequencing data for these *C. elegans* strains have been deposited at the NIH Sequence
503 Read Archive (SRA) under accession PRJNA1208078.
504 **CRIPSR/Cas9-derived stains:**
505 USD1042, *sulp-4(rae334) V*
506 <u>Chemical mutagenesis and whole genome sequencing:</u>
507 To define *C. elegans* gene activities that were necessary for promoting purine homeostasis, we
508 carried out a chemical mutagenesis screen for mutations that enhanced the penetrance of xanthine stone
509 formation in *xdh-1(ok3234)* mutant *C. elegans* (USD869). *C. elegans* were mutagenized with ethyl
510 methanesulfonate (EMS) using established protocols [20]. F2 generation animals that displayed a
511 xanthine stone were cloned onto individual NGM petri dishes, and F3 generation animals were screened
512 qualitatively for a population-level increase in xanthine stone penetrance. We demanded that new mutant
513 strains of interest were viable and fertile.
514 Here we report the analysis of 5 new mutant strains (USD962, USD971, USD990, USD1013, and
515 USD1019). Each of these strains carried new EMS-induced lesions (*rae299, rae302, rae319, rae320,* or
516 *rae326)* that enhanced the formation of xanthine stones in an *xdh-1* mutant background. Each mutation
517 was recessive; when heterozygous, each lesion caused 5% (*rae302, n*=42 individuals), 0% (*rae319, n*=38
518 individuals), 2% (*rae299, n*=41 individuals), or 5% (*rae326, n*=22 individuals) xanthine stone formation in

519 an *xdh-1* mutant background, dramatically reduced when compared to their homozygous counterparts
520 (**Fig. 2B)**. *rae320* was never characterized as dominant or recessive.
521 To further genetically analyze these lesions, we performed complementation analyses of these new
522 mutations. The *rae319* lesion failed to complement *rae302* (100% xanthine stone penetrance, *n*=71
523 individuals), *rae299* (87% xanthine stone penetrance, *n*=38 individuals), and *rae326* (100% xanthine stone
524 penetrance, *n*=14 individuals). All complementation experiments were performed in an *xdh-1(ok3234)*
525 homozygous mutant genetic background. These results suggest *rae302, rae319, rae299,* and *rae326* all
526 impact the same gene. Complementation studies were not performed on *rae320.*
527 To identify EMS-induced mutations in our strains of interest we followed established protocols [56].
528 Briefly, whole genomic DNA was prepared from *C. elegans* using the Gentra Puregene Tissue Kit (Qiagen)
529 and genomic DNA libraries were prepared using the NEBNext genomic DNA library construction kit (New
530 England Biolabs). DNA libraries were sequenced on an Illumina NovaSeq and deep sequencing reads
531 were analyzed using standard methods on Galaxy, a web-based platform for computational analyses [57].
532 Briefly, sequencing reads were trimmed and aligned to the WBcel235 *C. elegans* reference genome [58,
533 59]. Variations from the reference genome and the putative impact of those variations were annotated and
534 extracted for analysis [60-62]. All 4 strains that formed a complementation group possessed novel
535 mutations in the gene *sulp-4,* strongly suggesting that these lesions in *sulp-4* caused the enhanced
536 xanthine stone formation in the *xdh-1* mutant background (**Fig. 2A, Table S1**). Although the *rae320* lesion
537 found in USD1013 was not analyzed via complementation, whole genome sequence analyses identified a
538 homozygous mutation in *sulp-4*. Thus, we assume that the lesion in *sulp-4* found in USD1013 is also
539 causative for the enhanced xanthine stone formation in the *xdh-1* mutant background (**Table S1)**. In fact,
540 *rae319* and *rae320* are identical genetic lesions. We know that strains carrying these genetic lesions are
541 not siblings as they were derived from independent rounds of mutagenesis. Whole genome sequencing
542 data for these *C. elegans* strains have been deposited at the NIH Sequence Read Archive (SRA) under
543 accession PRJNA1208078.
544 <u>CRISPR/Cas9 genome editing:</u>
545 Genome engineering using CRISPR/Cas9 technology was performed using established techniques
546 [21, 22]. Briefly, 2 guide RNAs were designed and synthesized (IDT, crRNA) that targeted the *sulp-4* locus
547 (5'-agagttagctttgtacaacg-3' and 5'-atagcacatgatacttccgt-3'). Cas9 (IDT) guide RNA ribonucleoprotein
548 complexes were directly injected into the *C. elegans* germline [21]. Newly induced deletions were
549 identified in the offspring of injected animals using a PCR-based screening approach. The DNA primers
550 used to screen for new deletions were: 5'-gcagagaaactcagagcaacaa-3' and 5'- gcttggtttggaaactttgg-3'. We
551 were able to isolate and homozygoze *sulp-4(rae334),* a new deletion of *sulp-4* (**Fig. 2A**).
552 <u>*C. elegans* transgenesis:</u>
553 Transgenic *C. elegans* carrying extrachromosomal arrays were generated by micro-injecting the
554 gonad of young adult *xdh-1(ok3234); sulp-4(rae319)* double mutant *C. elegans* with an injection mix
555 consisting of the *Psulp-4::SULP-4::GFP* plasmid (20 ng/μl), the *Pmyo-2::mCherry* co-injection marker (2

556 ng/μl), and the KB+ ladder (78 ng/μl, New England Biolabs) [63]. Three independently derived transgenic
557 strains carrying the extrachromosomal arrays *raeEx118, raeEx119,* or *raeEx120* were isolated and
558 maintained by propagating individual animals based on expression of the fluorescent mCherry protein in
559 the pharynx.

560 Determination of xanthine stone penetrance:

561 To determine the percentage of animals that developed a xanthine stone, we cultured wild-type,
562 mutant, and transgenic *C. elegans* beginning at the L4 stage of development under various growth
563 conditions. Animals were assessed daily for the formation of stones and transferred to fresh petri dishes
564 (to avoid contamination from the subsequent generation) over the first 4 days of adulthood except for
565 experiments that used the *cdo-1(mg622)* allele where assays were terminated at day 3 of adulthood. *cdo-*
566 *1(mg622)* caused early lethality that limited the number of individuals that survived per biological replicate.
567 Thus, the assay was shortened to increase the sample size in **Fig. 1B, 5B, 6B, and S4A**. Importantly, all
568 datapoints in a given figure panel were subjected to the same assay conditions and are thus directly
569 comparable. Xanthine stones were determined based upon presence of exceptionally bright
570 autofluorescent puncta that were opaque when observed by brightfield microscopy. If an individual
571 displayed a stone, it was counted and removed from the assay. If an animal did not display a stone, it was
572 counted and moved to a fresh petri dish to prevent contamination from the subsequent generation and
573 allow for assessment on the following day. Xanthine stone penetrance was the percentage of animals that
574 displayed stone over the course of the assay. If animals went missing or died before the end of the assay,
575 they were not included in the final analyses.

576 *C. elegans* larval development and embryonic viability assays:

577 To assay developmental rates, *C. elegans* were synchronized at the first stage of larval
578 development. To synchronize animals, embryos were harvested from gravid adult animals via treatment
579 with a bleach and sodium hydroxide solution. Embryos were then incubated overnight in M9 solution
580 causing them to hatch and arrest development at the L1 stage [64]. Synchronized L1 animals were
581 cultured for 72 hours, and live animals were imaged as described below. Animal length was measured
582 from tip of head to the end of the tail.

583 To determine the hatching rate of wild-type and mutant *C. elegans,* we performed synchronized
584 egg lays using young adult animals. Embryos were then scored for hatching ~24 hours after being laid.

585 Microscopy:

586 Low magnification bright field and fluorescence images (**Fig. 1C, S1, and S3B-D**) were collected
587 using a Nikon SMZ25 microscope equipped with a Hamamatsu Orca flash 4.0 digital camera using NIS-
588 Elements software (Nikon). High magnification differential interference contrast (DIC) and GFP
589 fluorescence images (**Fig. 2C and 4A,B**) were collected using a Nikon NiE microscope equipped with a
590 Hamamatsu Orca flash 4.0 digital camera using NIS-Elements software (Nikon). All images were
591 processed and analyzed using ImageJ software (NIH). All imaging was performed on live animals
592 paralyzed using sodium azide.

593 Quantitative PCR (qPCR):

594 RNA was extracted from synchronized wild-type, *sulp-4(rae319),* and *osm-8(n1518)* young adult
595 animals using Trizol Reagent per manufacturer's instructions (Invitrogen). Prior to RNA extraction, live *C.*
596 *elegans* samples were washed and subsequently incubated for one hour in buffer M9 to allow for removal
597 of bacterial contamination. cDNA was then synthesized using the GoScript Reverse Transcriptase System
598 following manufacturer's instructions (Promega). qPCR was performed using a CFX96 Real-Time System
599 (Bio-Rad) and SYBR Green Master Mix following manufacturer's instructions (Applied Biosystems).
600 Relative mRNA levels were calculated using the comparative C_T methods [65]. Forward and reverse
601 amplification primers were: *act-1,* 5'-ctcttgccccatcaaccatg-3' and 5'-cttgcttggagatccacatc-3'; *cdo-1,* 5'-
602 ttcgatgagagaaccggaaag-3' and 5'-gccattcttagatcctctgtagtc-3'; *hmit-1.1,* 5'-ccattgaagaggtagaaatgc-3' and
603 5'-tgtacttcattgtgttgtcc-3'; and *gpdh-1,* 5'-tgcagagattccaggaaaccagg-3' and 5'-ccctttgtagcttgccacggag-3'.
604

605 **Acknowledgements:**

606 Some *C. elegans* strains were provided by the CGC, which is funded by the NIH Office of
607 Research Infrastructure Programs (P40 OD010440). We thank the lab of Emily Troemel for providing a *C.*
608 *elegans* strain carrying the *pnp-1(jy121)* mutation. We thank the lab of Keith Nehrke for providing the
609 *Psulp-4::SULP-4::GFP* plasmid (pTS1). Research reported in this publication was supported by the
610 National Institute of General Medical Sciences of the National Institutes of Health under award number
611 R35 GM146871 (to K.W.). A.V.A. was supported by the National Science Foundation Division of Biological
612 Infrastructure under award number 1756912. C.B. was supported by the National Institute of Childhood
613 Health and Human Development of the National Institutes of Health under award number R25 HD097633.
614
615
616
617
618
619
620
621
622
623
624
625
626
627
628
629

630 **Figures:**

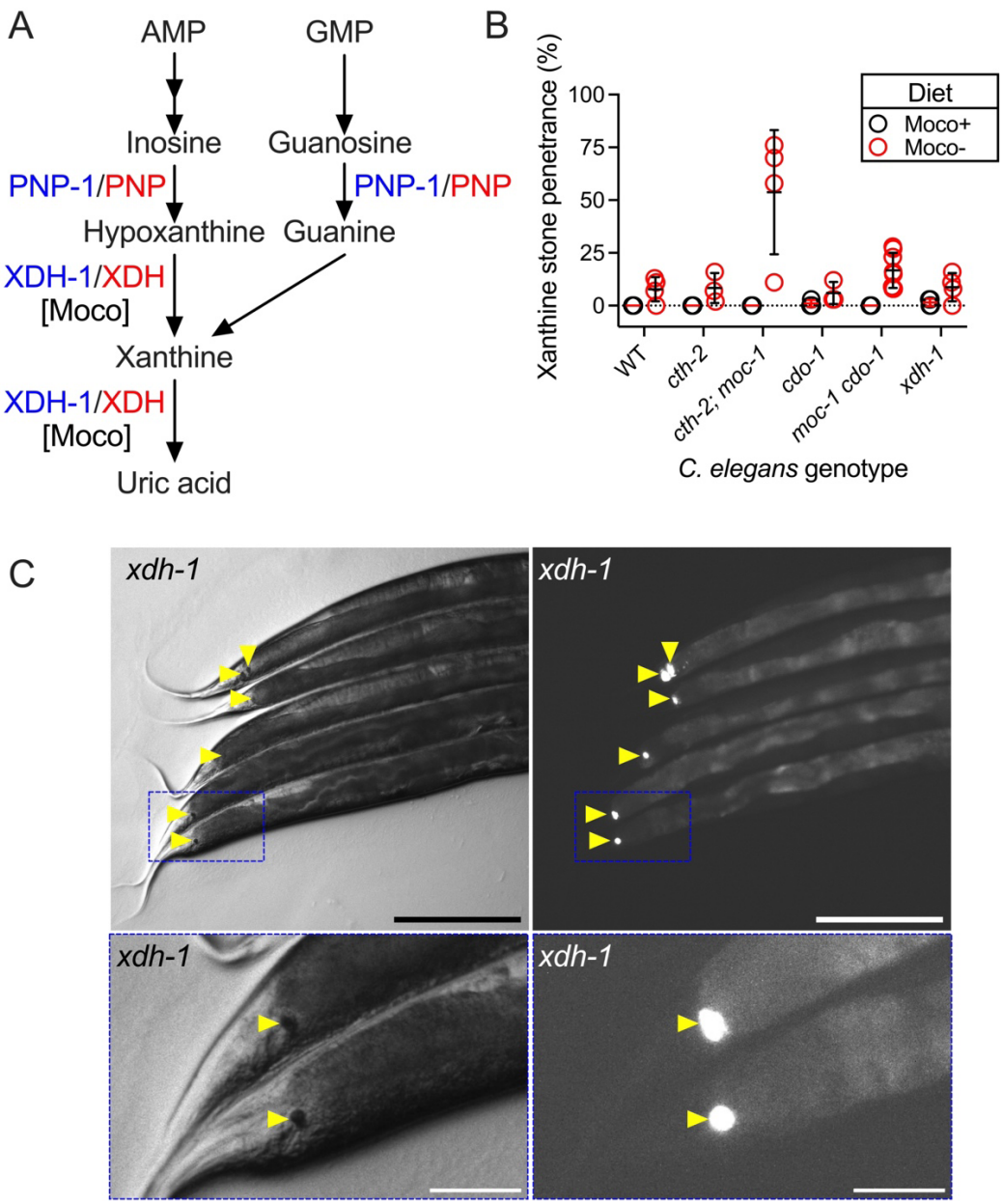

631

632 **Figure 1:** Moco deficiency or loss of *xdh-1* promoted the formation of autofluorescent xanthine stones.
633 A) Purine catabolism pathway. We highlight the roles of purine nucleoside phosphorylase (PNP-1/PNP),
634 and the Moco-requiring enzyme xanthine dehydrogenase (XDH-1/XDH). *C. elegans* enzymes (blue) and
635 their human homologs (red) are displayed. B) Wild-type and mutant *C. elegans* were cultured on wild-type
636 (black, Moco+) or *ΔmoaA* mutant (red, Moco-) *E. coli* and assessed for the formation of xanthine stones
637 over the first 3 days of adulthood. Individual data points represent biological replicates. Mean and
638 standard deviation are displayed. Complete information regarding sample size and individuals scored per
639 biological replicate are found in **Table S2**. C) Brightfield (left) and fluorescent (right) images of the
640 posterior of *xdh-1(ok3234)* mutant adult *C. elegans* cultured on wild-type *E. coli.* Xanthine stones are
641 highlighted (yellow arrowheads). The blue box indicates the region magnified in the lower panels. Scale
642 bar is 250μm (top) or 50μm (bottom).

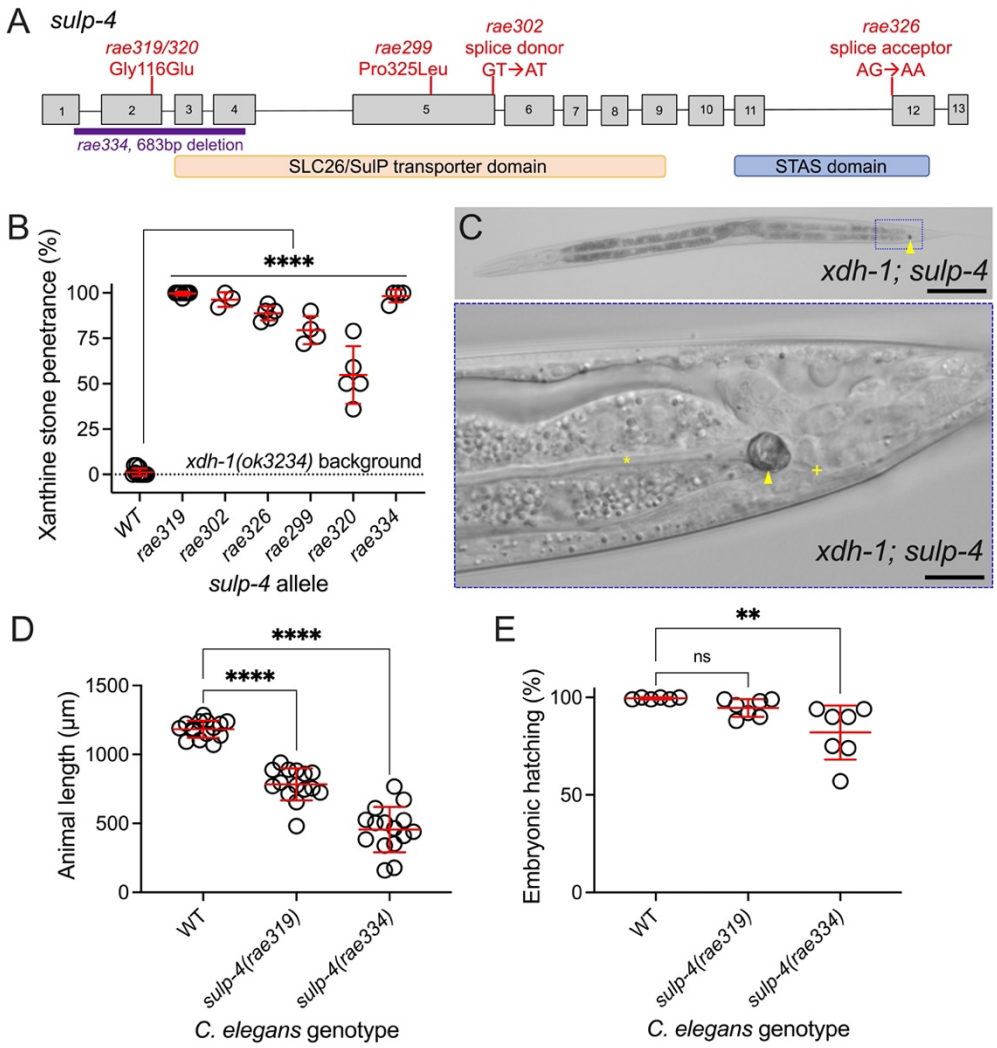

Figure 2: Loss-of-function mutations in *sulp-4* enhanced the formation of xanthine stones during *xdh-1* deficiency.

A) *sulp-4* locus. Gray boxes are exons and lines are introns. The regions that encode the SLC26/SulP sulfate permease domain (orange) and STAS domain (blue) are displayed. Red lines display the location of new EMS-induced lesions that enhance the formation of xanthine stones in an *xdh-1(ok3234)* mutant background. *rae334* (purple) is a deletion allele generated using CRISPR/Cas9 technology. B) Xanthine stone formation was assessed for *xdh-1(ok3234)* mutant *C. elegans* with wild-type (WT) or mutant *sulp-4(rae319, rae302, rae326, rae299, rae320,* or *rae334).* ****, p<0.0001, ordinary one-way ANOVA. Individual data points represent biological replicates. Mean and standard deviation are displayed. Complete information regarding sample size and individuals scored per biological replicate are found in **Table S2**. C) Differential interference contrast image of *xdh-1(ok3234); sulp-4(rae319) C. elegans* at the L4 stage of development. Blue box indicates the region magnified in the lower panel. Yellow arrowhead identifies the xanthine stone. Yellow asterisk identifies the lumen of the intestine. Yellow plus sign identifies the rectum. Scale bars are 100µm (top) and 10µm (bottom). D) Wild-type, *sulp-4(rae319),* and *sulp-4(rae334)* mutant *C. elegans* were synchronized at the first stage of larval development and cultured for 72 hours on wild-type *E. coli.* Animal length was determined. Individual datapoints are displayed as are the mean and standard deviation. The sample size is 15 individuals per genotype. ****, p<0.0001, ordinary one-way ANOVA. E) The hatching rate of newly laid wild-type, *sulp-4(rae319),* and *sulp-4(rae334)* mutant *C. elegans* embryos was determined. Individual data points represent biological replicates. Mean and standard deviation are displayed. Complete information regarding sample size and individuals scored per biological replicate are found in **Table S2**. **, p<0.01 or ns, p>0.05, ordinary one-way ANOVA.

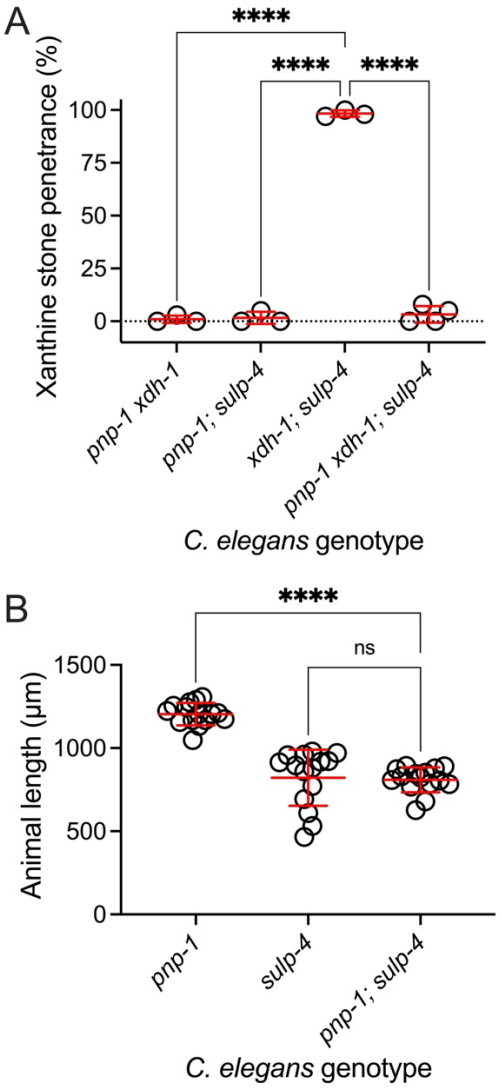

Figure 3: *pnp-1* was required for xanthine stone formation displayed by *xdh-1; sulp-4* mutants but not the larval delay caused by *sulp-4* loss of function.

A) Double and triple mutant *C. elegans* were assessed for xanthine stone formation when cultured on wild-type *E. coli*. ****, p<0.0001, ordinary one-way ANOVA. Individual data points represent biological replicates. Mean and standard deviation are displayed. Complete information regarding sample size and individuals scored per biological replicate are found in **Table S2**. B) *pnp-1(jy121), sulp-4(rae319),* and *pnp-1(jy121); sulp-4(rae319)* mutant *C. elegans* were synchronized at the first stage of larval development and cultured for 72 hours on wild-type *E. coli.* Animal length was determined. Individual datapoints are displayed as are the mean and standard deviation. The sample size is 15 individuals per genotype. ****, p<0.0001 or ns, p>0.05, ordinary one-way ANOVA.

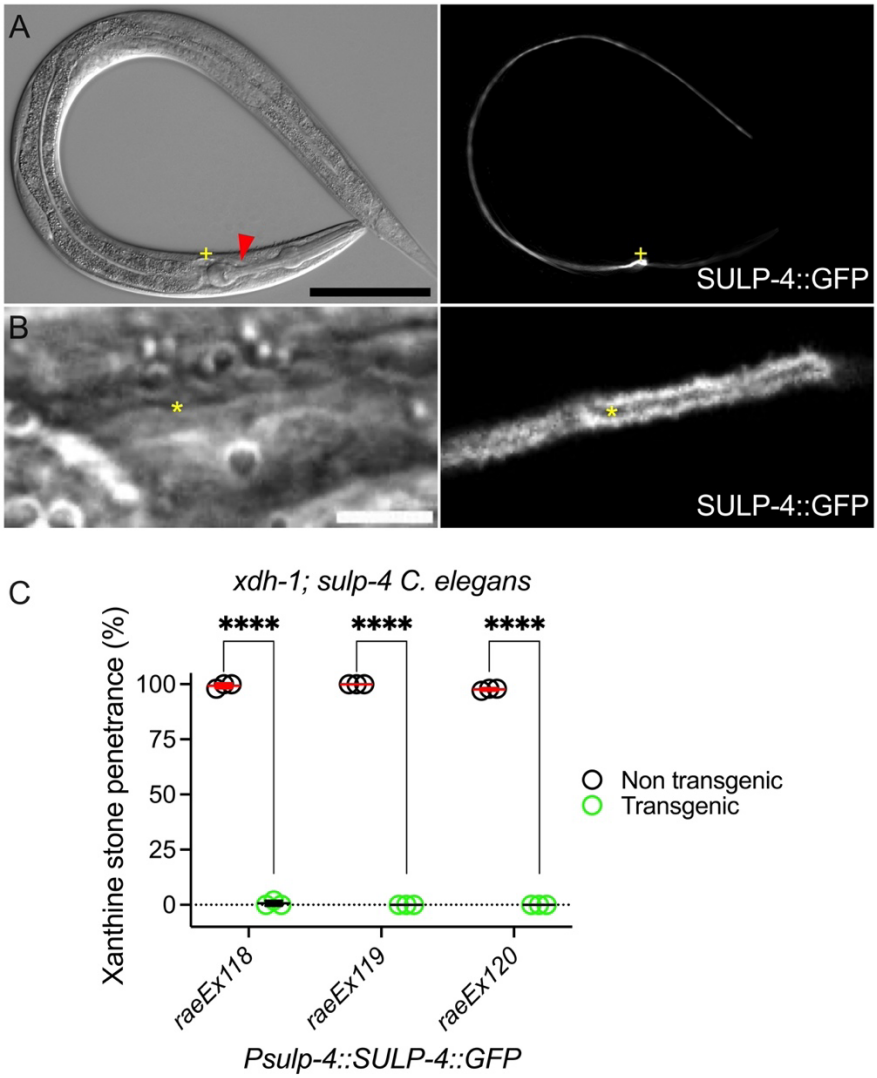

Figure 4: *sulp-4* acted cell non-autonomously in the excretory cell to limit xanthine stone formation. A,B) Differential interference contrast (left) and fluorescence imaging (right) of *xdh-1(ok3234); sulp-4(rae319) C. elegans* expressing the *Psulp-4::SULP-4::GFP* transgene (SULP-4::GFP). Yellow plus sign identifies the cell body of the excretory cell. Red arrow indicates the region magnified in panel B. Yellow asterisk identifies the lumen of the excretory cell. Scale bars are 100μm (A, top) and 5μm (B, bottom). C) Transgenic *xdh-1(ok3234); sulp-4(rae319) C. elegans* expressing the *Psulp-4::SULP-4::GFP* transgene (green) and their non-transgenic siblings (black) were assessed for the formation of xanthine stones. Individual data points represent biological replicates. Mean and standard deviation are displayed. ****, $p<0.0001$, multiple unpaired t tests. Complete information regarding sample size and individuals scored per biological replicate are found in **Table S2**.

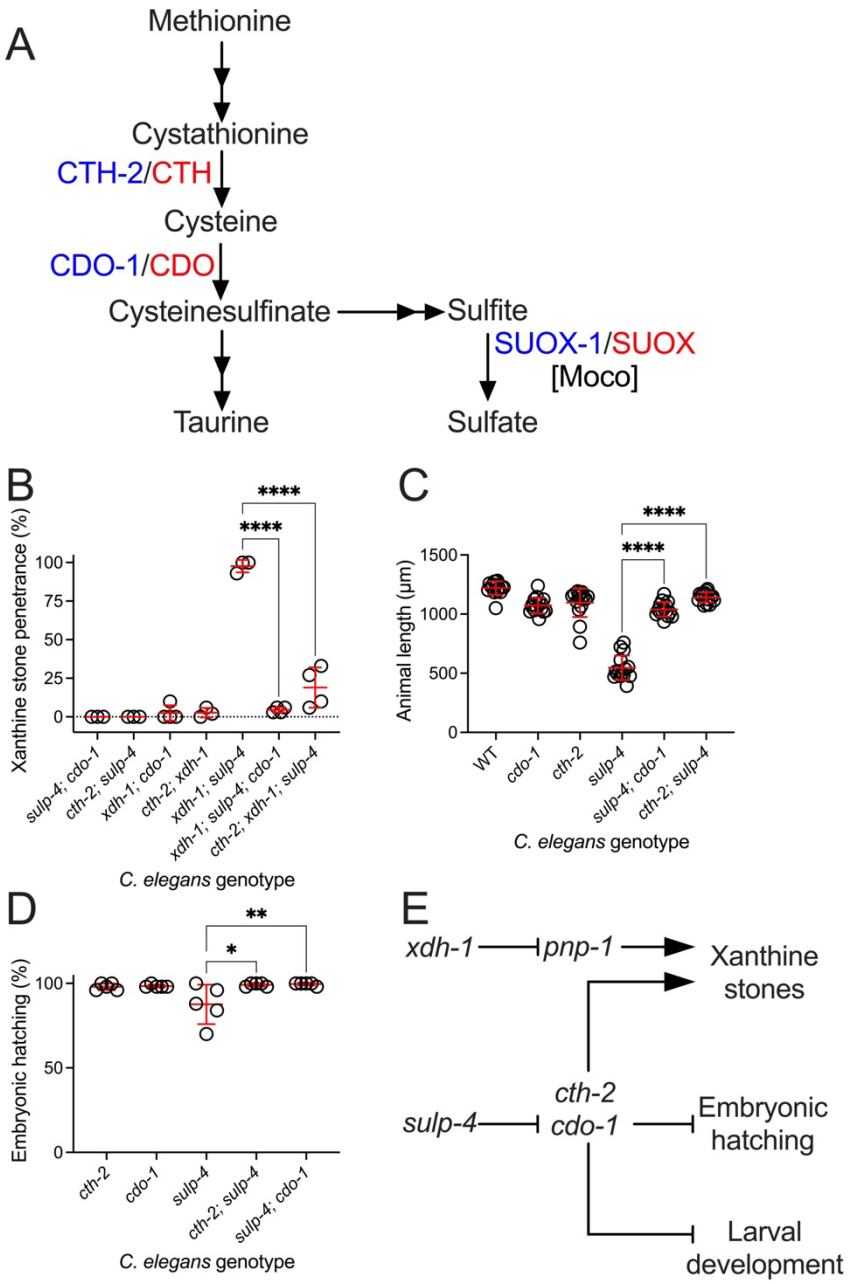

Figure 5: *cth-2* and *cdo-1* were required for phenotypes caused by *sulp-4* loss of function. A) Sulfur amino acid catabolism pathway. We highlight the roles of cystathionase (CTH-2/CTH), cysteine dioxygenase (CDO-1/CDO), and the Moco-requiring enzyme sulfite oxidase (SUOX-1/SUOX). *C. elegans* enzymes (blue) and their human homologs (red) are displayed. B) Double and triple mutant *C. elegans* were assessed for xanthine stone formation when cultured on wild-type *E. coli* over the first 3 days of adulthood. Individual data points represent biological replicates. Mean and standard deviation are displayed. ****, p<0.0001, ordinary one-way ANOVA. Complete information regarding sample size and individuals scored per biological replicate are found in **Table S2**. C) Wild-type and mutant *C. elegans* were synchronized at the first stage of larval development and cultured for 72 hours on wild type *E. coli.* Animal length was determined. Individual datapoints are displayed as are the mean and standard deviation. The sample size is 15 individuals per genotype. ****, p<0.0001, ordinary one-way ANOVA. D) The hatching rate of newly laid single and double mutant *C. elegans* embryos was determined. Individual data points represent biological replicates. Mean and standard deviation are displayed. **, p<0.01 or *, p<0.05, ordinary one-way ANOVA. Complete information regarding sample size and individuals scored per biological replicate are found in **Table S2**. The *sulp-4(rae334)* allele was used to generate the data in **Fig. 5B-D.** E) A genetic pathway outlining the roles of *xdh-1, pnp-1, sulp-4, cth-2,* and *cdo-1* in governing xanthine stone formation, embryonic hatching, and larval development.

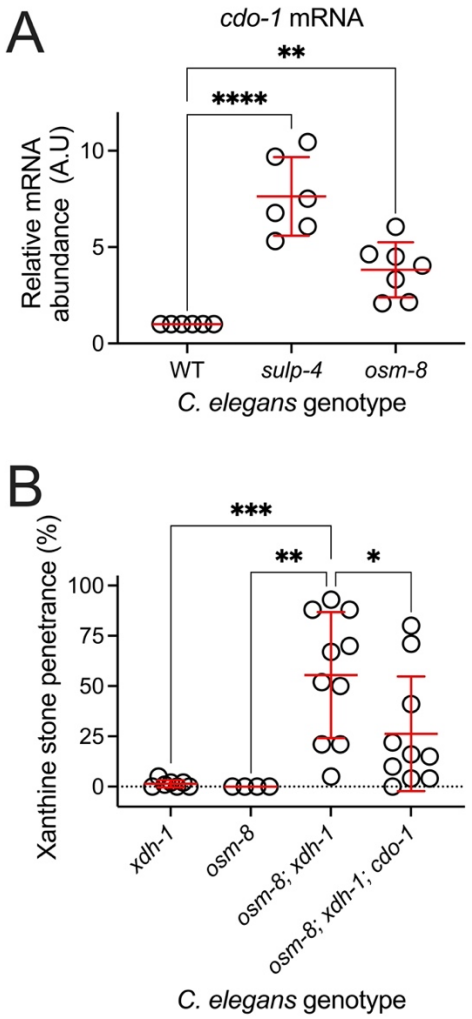

Figure 6: Loss of *osm-8,* which activates the osmotic stress response, enhanced xanthine stone accumulation in *xdh-1* mutant *C. elegans.*

A) Relative mRNA levels of *cdo-1* are displayed for total RNA isolated from wild-type, *sulp-4(rae319)*, and *osm-8(n1518)* young adult *C. elegans.* Relative mRNA abundance was determined via the delta-delta C_T method. All transcripts are normalized to *act-1.* Relative mRNA abundance for each transcript was set to one in the wild type. ****, $p<0.0001$, **, $p<0.01$, ordinary one-way ANOVA. B) Mutant *C. elegans* were assessed for xanthine stone formation when cultured on wild-type *E. coli*. Individual data points represent biological replicates. Mean and standard deviation are displayed. ***, $p<0.001$, **, $p<0.01$, *, $p<0.05$, ordinary one-way ANOVA. Complete information regarding sample size and individuals scored per biological replicate are found in **Table S2**.

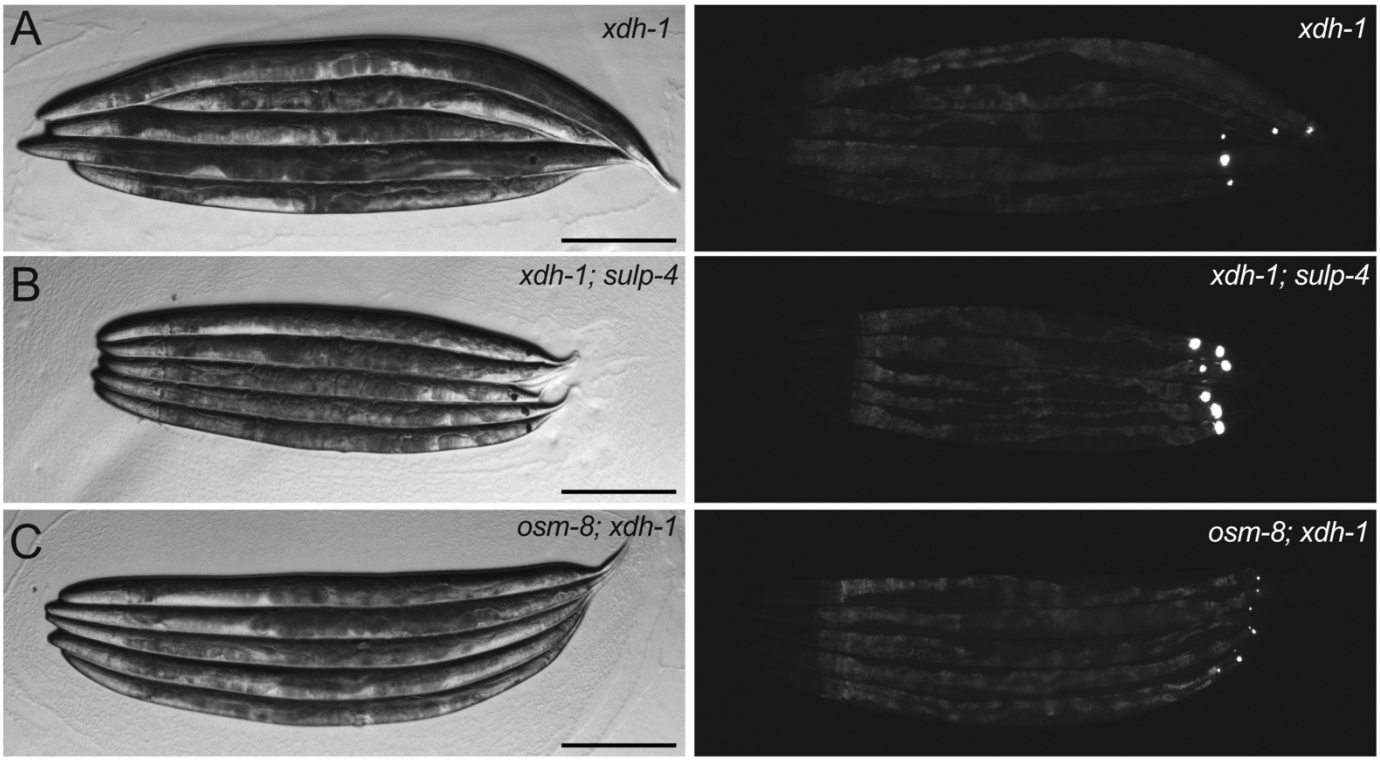

Supplementary Figure 1: Loss of *sulp-4* enhanced the expressivity of the xanthine stone phenotype displayed by *xdh-1* mutant animals.

Brightfield (left) and fluorescent (right) images of the posterior of A) *xdh-1(ok3234)* and B) *xdh-1(ok3234); sulp-4(rae319)* or C) *osm-8(n1518); xdh-1(ok3234)* mutant adult *C. elegans* cultured on wild-type *E. coli.* Scale bar is 250μm. Note, *xdh-1(ok3234)* animals displayed are older than their *xdh-1(ok3234); sulp-4(rae319)* or *osm-8(n1518); xdh-1(ok3234)* counterparts which were imaged as day 2 adults. This was necessary to allow us to identify sufficient *xdh-1* single mutant animals displaying a xanthine stone.

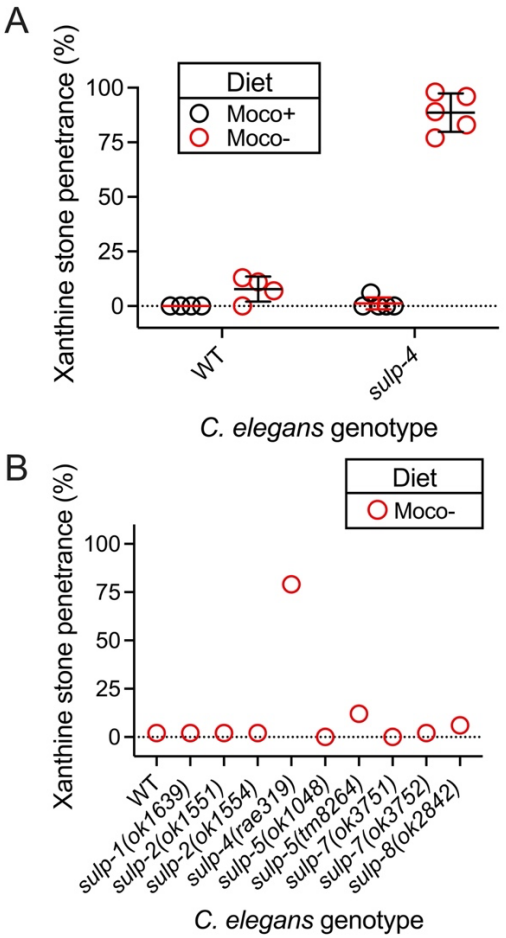

Supplementary Figure 2: Inactivating mutations in *sulp* genes other than *sulp-4* did not enhance xanthine stone formation during dietary Moco deficiency.

A) Wild-type and *sulp-4(rae319) C. elegans* were cultured on wild-type (black, Moco+) or *ΔmoaA* mutant (red, Moco-) *E. coli* and assessed for the formation of xanthine stones. Note, data points for the wild-type animals cultured on Moco+ and Moco- *E. coli* are derived from the same experiment that is displayed in Figure 1B. However, in this analysis the animals were scored until day 4 of adulthood. B) Wild type and viable *sulp* mutant *C. elegans* were cultured on *ΔmoaA* mutant (red, Moco-) *E. coli* and assessed for the formation of xanthine stones. Data points represent a single biological replicate with 19-53 individuals per replicate. Complete information regarding individuals scored per biological replicate are found in **Table S2**.

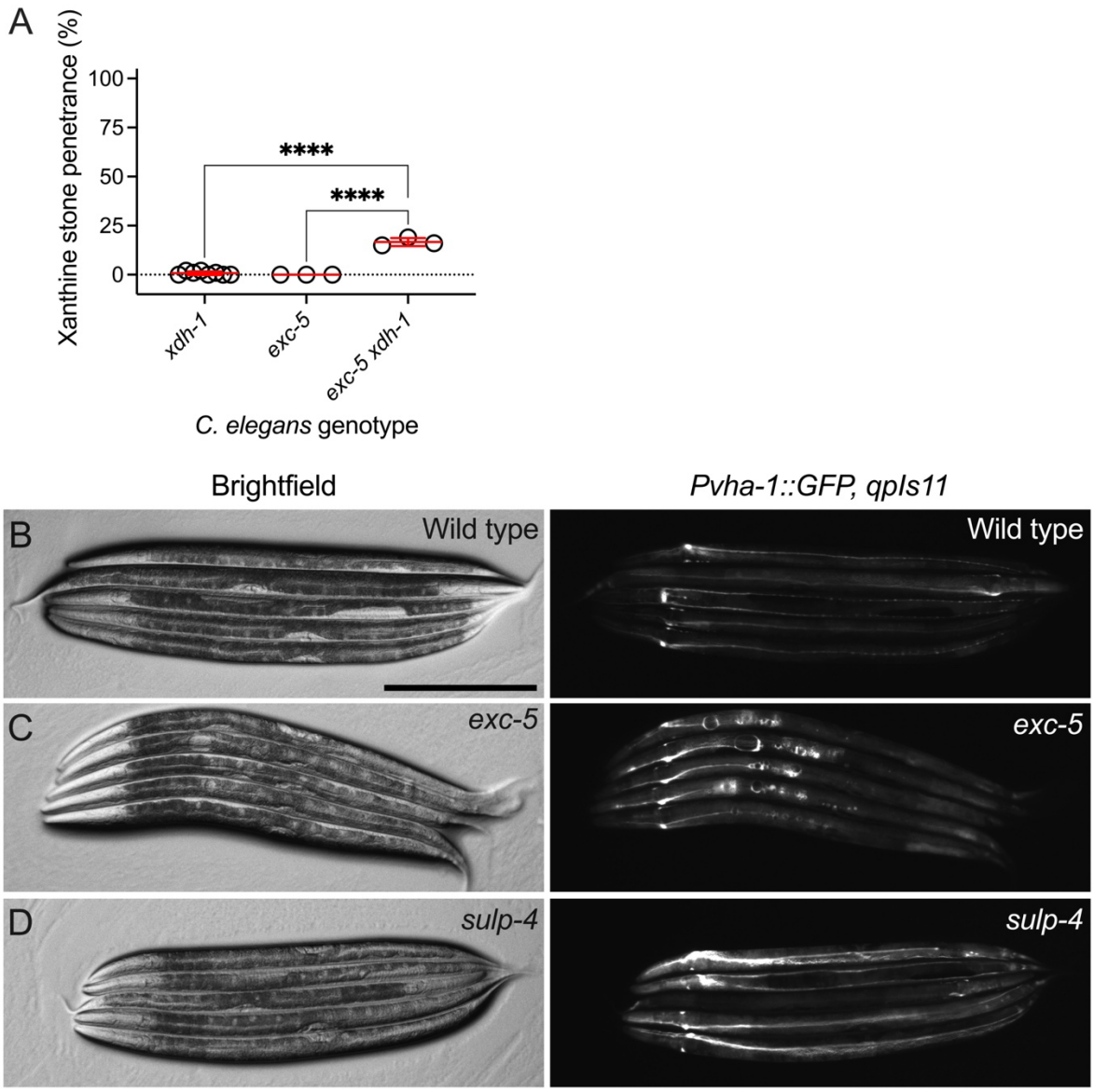

Supplementary Figure 3: Loss of *exc-5* modestly enhanced the formation of xanthine stones in an *xdh-1* mutant background while *sulp-4* loss of function does not impact excretory cell morphology. A) *xdh-1(ok3234), exc-5(rh232),* and *exc-5(rh232) xdh-1(ok3234)* mutant *C. elegans* were assessed for xanthine stone formation when cultured on wild-type *E. coli*. Individual data points represent biological replicates. Mean and standard deviation are displayed. ****, $p<0.0001$, ordinary one-way ANOVA. Complete information regarding sample size and individuals scored per biological replicate are found in **Table S2**. B-D) Brightfield (left) and fluorescence imaging (right) are displayed for B) wild-type, C) *exc-5(rh232),* or D) *sulp-4(rae319) C. elegans* expressing the *qpIs11* (*Pvha-1::GFP)* transgene, which marks the excretory cell. Scale bar is 250μm

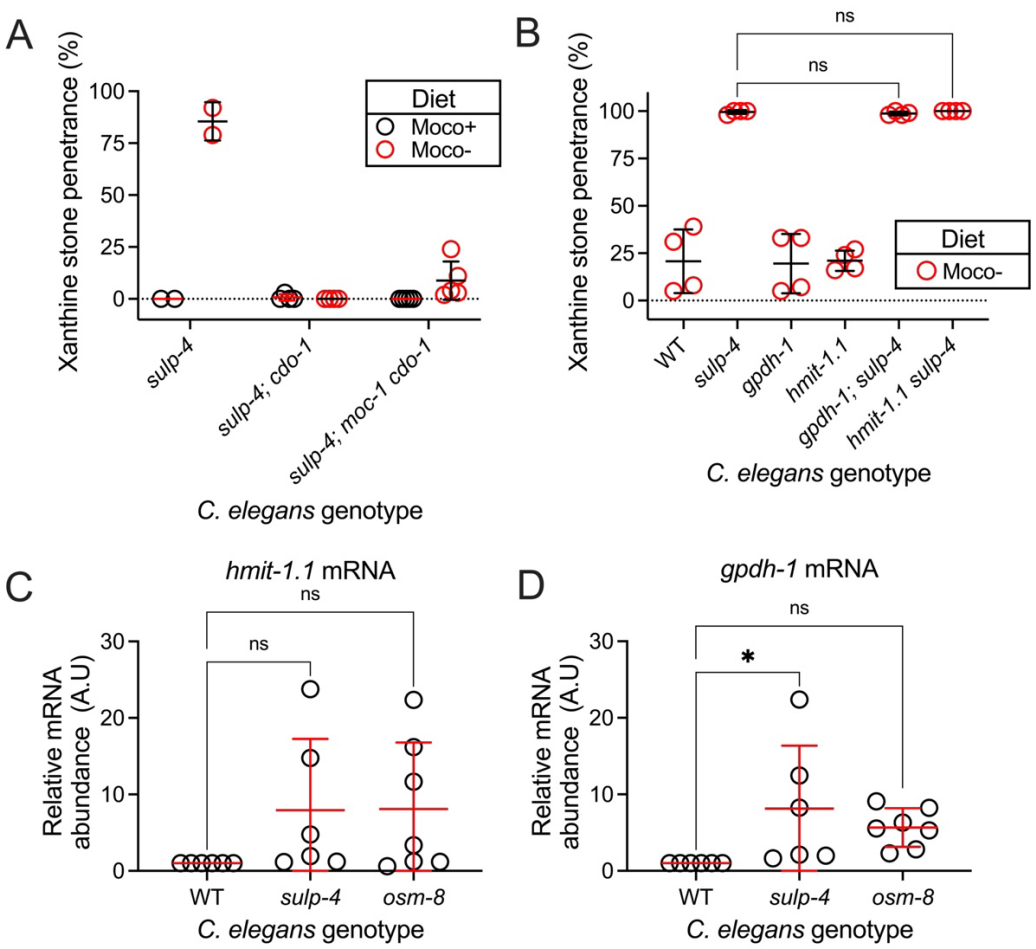

Supplementary Figure 4: *cdo-1,* but not *hmit-1.1* or *gpdh-1,* was necessary for the enhanced formation of xanthine stones caused by *sulp-4* inactivation during dietary Moco deficiency.

A) *sulp-4(rae319), sulp-4(rae319); cdo-1(mg622),* and *sulp-4(rae319); moc-1(ok366) cdo-1(mg622)* mutant *C. elegans* were cultured on wild-type (black, Moco+) or *ΔmoaA* mutant (red, Moco-) *E. coli* and assessed for the formation of xanthine stones over the first 3 days of adulthood. B) Wild type and mutant *C. elegans* were cultured on *ΔmoaA* mutant (red, Moco-) *E. coli* and assessed for the formation of xanthine stones. Individual data points represent biological replicates. Mean and standard deviation are displayed. ns, p>0.05, ordinary one-way ANOVA. Complete information regarding sample size and individuals scored per biological replicate are found in **Table S2**. Relative mRNA expression of C) *hmit-1.1* and D) *gpdh-1* are displayed for total RNA isolated from wild-type, *sulp-4(rae319)*, and *osm-8(n1518)* young adult *C. elegans.* Relative mRNA abundance was determined via the delta-delta C_T method. All transcripts are normalized to *act-1.* Relative mRNA abundance for each transcript was set to one in the wild type. *, p<0.05, ns, p>0.05, ordinary one-way ANOVA.

Strain	Allele	Chromosome	Chromosome position	Gene affected	Reference base	Mutant base	Allele status	Variant impact
USD962	*rae299*	V	11876913	*sulp-4*	C	T	Homozygous	Pro325Leu
USD971	*rae302*	V	11877161	*sulp-4*	G	A	Homozygous	Splice donor variant
USD990	*rae319*	V	11875799	*sulp-4*	G	A	Homozygous	Gly116Glu
USD1013	*rae320*	V	11875799	*sulp-4*	G	A	Homozygous	Gly116Glu
USD1019	*rae326*	V	11878726	*sulp-4*	G	A	Homozygous	Splice acceptor variant

Supplementary Table 1: EMS-induced lesions in *sulp-4* that promoted the formation of xanthine stones in *xdh-1(ok3234)*-mutant *C. elegans.*

Supplementary Table 2: Raw data and information regarding sample sizes and biological replicates.

Literature cited:

1. Mullen NJ, Singh PK. Nucleotide metabolism: a pan-cancer metabolic dependency. Nat Rev Cancer. 2023;23(5):275-94. Epub 2023/03/28. doi: 10.1038/s41568-023-00557-7. PubMed PMID: 36973407; PubMed Central PMCID: PMCPMC10041518.
2. Lesch M, Nyhan WL. A FAMILIAL DISORDER OF URIC ACID METABOLISM AND CENTRAL NERVOUS SYSTEM FUNCTION. Am J Med. 1964;36:561-70. Epub 1964/04/01. doi: 10.1016/0002-9343(64)90104-4. PubMed PMID: 14142409.
3. Giblett ER, Ammann AJ, Wara DW, Sandman R, Diamond LK. Nucleoside-phosphorylase deficiency in a child with severely defective T-cell immunity and normal B-cell immunity. Lancet. 1975;1(7914):1010-3. Epub 1975/05/03. doi: 10.1016/s0140-6736(75)91950-9. PubMed PMID: 48676.
4. Duran M, Beemer FA, van de Heiden C, Korteland J, de Bree PK, Brink M, et al. Combined deficiency of xanthine oxidase and sulphite oxidase: a defect of molybdenum metabolism or transport? J Inherit Metab Dis. 1978;1(4):175-8. Epub 1978/01/01. doi: 10.1007/bf01805591. PubMed PMID: 117254.
5. Dent CE, Philpot GR. Xanthinuria, an inborn error (or deviation) of metabolism. Lancet. 1954;266(6804):182-5. Epub 1954/01/23. doi: 10.1016/s0140-6736(54)91257-x. PubMed PMID: 13118765.
6. Ball EG. XANTHINE OXIDASE: PURIFICATION AND PROPERTIES. J Biol Chem. 1939;128(1):51-67.
7. Sebesta I. Genetic disorders resulting in hyper- or hypouricemia. Adv Chronic Kidney Dis. 2012;19(6):398-403. Epub 2012/10/24. doi: 10.1053/j.ackd.2012.06.002. PubMed PMID: 23089275.
8. Warnhoff K, Ruvkun G. Molybdenum cofactor transfer from bacteria to nematode mediates sulfite detoxification. Nat Chem Biol. 2019;15(5):480-8. Epub 2019/03/27. doi: 10.1038/s41589-019-0249-y. PubMed PMID: 30911177; PubMed Central PMCID: PMCPMC6470025.
9. Schwarz G, Mendel RR, Ribbe MW. Molybdenum cofactors, enzymes and pathways. Nature. 2009;460(7257):839-47. Epub 2009/08/14. doi: 10.1038/nature08302. PubMed PMID: 19675644.
10. Snoozy J, Breen PC, Ruvkun G, Warnhoff K. moc-6/MOCS2A is necessary for molybdenum cofactor synthesis in C. elegans. MicroPubl Biol. 2022;2022. Epub 2022/03/01. doi: 10.17912/micropub.biology.000531. PubMed PMID: 35224462; PubMed Central PMCID: PMCPMC8864482.
11. Warnhoff K, Hercher TW, Mendel RR, Ruvkun G. Protein-bound molybdenum cofactor is bioavailable and rescues molybdenum cofactor-deficient C. elegans. Genes Dev. 2021;35(3-

4):212-7. Epub 2021/01/16. doi: 10.1101/gad.345579.120. PubMed PMID: 33446569; PubMed Central PMCID: PMCPMC7849362.
12. Oliphant KD, Fettig RR, Snoozy J, Mendel RR, Warnhoff K. Obtaining the necessary molybdenum cofactor for sulfite oxidase activity in the nematode Caenorhabditis elegans surprisingly involves a dietary source. J Biol Chem. 2023;299(1):102736. Epub 2022/11/25. doi: 10.1016/j.jbc.2022.102736. PubMed PMID: 36423681; PubMed Central PMCID: PMCPMC9793310.
13. Sherman T, Chernova MN, Clark JS, Jiang L, Alper SL, Nehrke K. The abts and sulp families of anion transporters from Caenorhabditis elegans. Am J Physiol Cell Physiol. 2005;289(2):C341-51. Epub 2005/04/09. doi: 10.1152/ajpcell.00071.2005. PubMed PMID: 15814591.
14. Nelson FK, Riddle DL. Functional study of the Caenorhabditis elegans secretory-excretory system using laser microsurgery. J Exp Zool. 1984;231(1):45-56. Epub 1984/07/01. doi: 10.1002/jez.1402310107. PubMed PMID: 6470649.
15. Chalmers RA, Watts RW, Pallis C, Bitensky L, Chayen J. Crystalline deposits in striped muscle in xanthinuria. Nature. 1969;221(5176):170-1. Epub 1969/01/11. doi: 10.1038/221170a0. PubMed PMID: 5782709.
16. Watts RW, Engelman K, Klinenberg JR, Seegmiller JE, Sjoerdsma A. ENZYME DEFECT IN A CASE OF XANTHINURIA. Nature. 1964;201:395-6. Epub 1964/01/25. doi: 10.1038/201395a0. PubMed PMID: 14110004.
17. Ma X, Wang W, Bittner F, Schmidt N, Berkey R, Zhang L, et al. Dual and Opposing Roles of Xanthine Dehydrogenase in Defense-Associated Reactive Oxygen Species Metabolism in Arabidopsis. Plant Cell. 2016;28(5):1108-26. Epub 2016/05/07. doi: 10.1105/tpc.15.00880. PubMed PMID: 27152019; PubMed Central PMCID: PMCPMC4904670.
18. Chi T, Kim MS, Lang S, Bose N, Kahn A, Flechner L, et al. A Drosophila model identifies a critical role for zinc in mineralization for kidney stone disease. PLoS One. 2015;10(5):e0124150. Epub 2015/05/15. doi: 10.1371/journal.pone.0124150. PubMed PMID: 25970330; PubMed Central PMCID: PMCPMC4430225.
19. Glassman E, Mitchell HK. Mutants of Drosophila Melanogaster Deficient in Xanthine Dehydrogenase. Genetics. 1959;44(2):153-62. Epub 1959/03/01. doi: 10.1093/genetics/44.2.153. PubMed PMID: 17247815; PubMed Central PMCID: PMCPMC1209939.
20. Brenner S. The genetics of Caenorhabditis elegans. Genetics. 1974;77(1):71-94. Epub 1974/05/01. PubMed PMID: 4366476; PubMed Central PMCID: PMCPMC1213120.
21. Cho SW, Lee J, Carroll D, Kim JS, Lee J. Heritable gene knockout in Caenorhabditis elegans by direct injection of Cas9-sgRNA ribonucleoproteins. Genetics. 2013;195(3):1177-80. Epub 2013/08/28. doi: 10.1534/genetics.113.155853. PubMed PMID: 23979576; PubMed Central PMCID: PMCPMC3813847.
22. Ghanta KS, Mello CC. Melting dsDNA Donor Molecules Greatly Improves Precision Genome Editing in Caenorhabditis elegans. Genetics. 2020;216(3):643-50. Epub 2020/09/24. doi: 10.1534/genetics.120.303564. PubMed PMID: 32963112; PubMed Central PMCID: PMCPMC7648581.
23. Tecle E, Chhan CB, Franklin L, Underwood RS, Hanna-Rose W, Troemel ER. The purine nucleoside phosphorylase pnp-1 regulates epithelial cell resistance to infection in C. elegans. PLoS Pathog. 2021;17(4):e1009350. Epub 2021/04/21. doi: 10.1371/journal.ppat.1009350. PubMed PMID: 33878133; PubMed Central PMCID: PMCPMC8087013.
24. Altschul SF, Gish W, Miller W, Myers EW, Lipman DJ. Basic local alignment search tool. J Mol Biol. 1990;215(3):403-10. Epub 1990/10/05. doi: 10.1016/s0022-2836(05)80360-2. PubMed PMID: 2231712.
25. Buechner M. Tubes and the single C. elegans excretory cell. Trends Cell Biol. 2002;12(10):479-84. Epub 2002/11/21. doi: 10.1016/s0962-8924(02)02364-4. PubMed PMID: 12441252.

26. Suzuki N, Buechner M, Nishiwaki K, Hall DH, Nakanishi H, Takai Y, et al. A putative GDP-GTP exchange factor is required for development of the excretory cell in Caenorhabditis elegans. EMBO Rep. 2001;2(6):530-5. Epub 2001/06/21. doi: 10.1093/embo-reports/kve110. PubMed PMID: 11415987; PubMed Central PMCID: PMCPMC1083904.
27. Warnhoff K, Bhattacharya S, Snoozy J, Breen PC, Ruvkun G. Hypoxia-inducible factor induces cysteine dioxygenase and promotes cysteine homeostasis in Caenorhabditis elegans. Elife. 2024;12. Epub 2024/02/13. doi: 10.7554/eLife.89173. PubMed PMID: 38349720.
28. Stipanuk MH, Ueki I. Dealing with methionine/homocysteine sulfur: cysteine metabolism to taurine and inorganic sulfur. J Inherit Metab Dis. 2011;34(1):17-32. Epub 2010/02/18. doi: 10.1007/s10545-009-9006-9. PubMed PMID: 20162368; PubMed Central PMCID: PMCPMC2901774.
29. Lee SD, Choi SY, Lim SW, Lamitina ST, Ho SN, Go WY, et al. TonEBP stimulates multiple cellular pathways for adaptation to hypertonic stress: organic osmolyte-dependent and -independent pathways. Am J Physiol Renal Physiol. 2011;300(3):F707-15. Epub 2011/01/07. doi: 10.1152/ajprenal.00227.2010. PubMed PMID: 21209002; PubMed Central PMCID: PMCPMC3064130.
30. Lamitina T, Huang CG, Strange K. Genome-wide RNAi screening identifies protein damage as a regulator of osmoprotective gene expression. Proc Natl Acad Sci U S A. 2006;103(32):12173-8. Epub 2006/08/02. doi: 10.1073/pnas.0602987103. PubMed PMID: 16880390; PubMed Central PMCID: PMCPMC1567714.
31. Lamitina ST, Morrison R, Moeckel GW, Strange K. Adaptation of the nematode Caenorhabditis elegans to extreme osmotic stress. Am J Physiol Cell Physiol. 2004;286(4):C785-91. Epub 2003/12/03. doi: 10.1152/ajpcell.00381.2003. PubMed PMID: 14644776.
32. Kage-Nakadai E, Uehara T, Mitani S. H+/myo-inositol transporter genes, hmit-1.1 and hmit-1.2, have roles in the osmoprotective response in Caenorhabditis elegans. Biochem Biophys Res Commun. 2011;410(3):471-7. Epub 2011/06/18. doi: 10.1016/j.bbrc.2011.06.001. PubMed PMID: 21679696.
33. Rohlfing AK, Miteva Y, Hannenhalli S, Lamitina T. Genetic and physiological activation of osmosensitive gene expression mimics transcriptional signatures of pathogen infection in C. elegans. PLoS One. 2010;5(2):e9010. Epub 2010/02/04. doi: 10.1371/journal.pone.0009010. PubMed PMID: 20126308; PubMed Central PMCID: PMCPMC2814864.
34. Rohlfing AK, Miteva Y, Moronetti L, He L, Lamitina T. The Caenorhabditis elegans mucin-like protein OSM-8 negatively regulates osmosensitive physiology via the transmembrane protein PTR-23. PLoS Genet. 2011;7(1):e1001267. Epub 2011/01/22. doi: 10.1371/journal.pgen.1001267. PubMed PMID: 21253570; PubMed Central PMCID: PMCPMC3017116.
35. Yanagi KS, Jochim B, Kunjo SO, Breen P, Ruvkun G, Lehrbach N. Mutations in nucleotide metabolism genes bypass proteasome defects in png-1/NGLY1-deficient Caenorhabditis elegans. PLoS Biol. 2024;22(7):e3002720. Epub 2024/07/11. doi: 10.1371/journal.pbio.3002720. PubMed PMID: 38991033; PubMed Central PMCID: PMCPMC11265709.
36. Ast T, Meisel JD, Patra S, Wang H, Grange RMH, Kim SH, et al. Hypoxia Rescues Frataxin Loss by Restoring Iron Sulfur Cluster Biogenesis. Cell. 2019;177(6):1507-21.e16. Epub 2019/04/30. doi: 10.1016/j.cell.2019.03.045. PubMed PMID: 31031004; PubMed Central PMCID: PMCPMC6911770.
37. Bantia S, Parker C, Upshaw R, Cunningham A, Kotian P, Kilpatrick JM, et al. Potent orally bioavailable purine nucleoside phosphorylase inhibitor BCX-4208 induces apoptosis in B- and T-lymphocytes--a novel treatment approach for autoimmune diseases, organ transplantation and hematologic malignancies. Int Immunopharmacol. 2010;10(7):784-90. Epub 2010/04/20. doi: 10.1016/j.intimp.2010.04.009. PubMed PMID: 20399911.

931 38. Kamath VP, Juarez-Brambila JJ, Morris PE, Jr. Synthesis of labeled BCX-4208, a potent
932 inhibitor of purine nucleoside phosphorylase. Drug Test Anal. 2009;1(3):125-7. Epub 2010/04/01.
933 doi: 10.1002/dta.24. PubMed PMID: 20355185.
934 39. Dorwart MR, Shcheynikov N, Yang D, Muallem S. The solute carrier 26 family of proteins
935 in epithelial ion transport. Physiology (Bethesda). 2008;23:104-14. Epub 2008/04/11. doi:
936 10.1152/physiol.00037.2007. PubMed PMID: 18400693.
937 40. Sindić A, Chang MH, Mount DB, Romero MF. Renal physiology of SLC26 anion
938 exchangers. Curr Opin Nephrol Hypertens. 2007;16(5):484-90. Epub 2007/08/19. doi:
939 10.1097/MNH.0b013e3282e7d7d0. PubMed PMID: 17693766.
940 41. Hill AJ, Basourakos SP, Lewicki P, Wu X, Arenas-Gallo C, Chuang D, et al. Incidence of
941 Kidney Stones in the United States: The Continuous National Health and Nutrition Examination
942 Survey. J Urol. 2022;207(4):851-6. Epub 2021/12/03. doi: 10.1097/ju.0000000000002331.
943 PubMed PMID: 34854755.
944 42. Moe OW. Kidney stones: pathophysiology and medical management. Lancet.
945 2006;367(9507):333-44. Epub 2006/01/31. doi: 10.1016/s0140-6736(06)68071-9. PubMed PMID:
946 16443041.
947 43. Jiang Z, Asplin JR, Evan AP, Rajendran VM, Velazquez H, Nottoli TP, et al. Calcium
948 oxalate urolithiasis in mice lacking anion transporter Slc26a6. Nat Genet. 2006;38(4):474-8. Epub
949 2006/03/15. doi: 10.1038/ng1762. PubMed PMID: 16532010.
950 44. Cornière N, Thomson RB, Thauvin S, Villoutreix BO, Karp S, Dynia DW, et al. Dominant
951 negative mutation in oxalate transporter SLC26A6 associated with enteric hyperoxaluria and
952 nephrolithiasis. J Med Genet. 2022;59(11):1035-43. Epub 2022/02/05. doi: 10.1136/jmedgenet-
953 2021-108256. PubMed PMID: 35115415; PubMed Central PMCID: PMCPMC9346097.
954 45. Gee HY, Jun I, Braun DA, Lawson JA, Halbritter J, Shril S, et al. Mutations in SLC26A1
955 Cause Nephrolithiasis. Am J Hum Genet. 2016;98(6):1228-34. Epub 2016/05/24. doi:
956 10.1016/j.ajhg.2016.03.026. PubMed PMID: 27210743; PubMed Central PMCID:
957 PMCPMC4908148.
958 46. Hirata T, Cabrero P, Berkholz DS, Bondeson DP, Ritman EL, Thompson JR, et al. In vivo
959 Drosophilia genetic model for calcium oxalate nephrolithiasis. Am J Physiol Renal Physiol.
960 2012;303(11):F1555-62. Epub 2012/09/21. doi: 10.1152/ajprenal.00074.2012. PubMed PMID:
961 22993075; PubMed Central PMCID: PMCPMC3532482.
962 47. Prince CL, Scardino PL, Wolan CT. The effect of temperature, humidity and dehydration on
963 the formation of renal calculi. J Urol. 1956;75(2):209-15. Epub 1956/02/01. doi: 10.1016/s0022-
964 5347(17)66798-3. PubMed PMID: 13296117.
965 48. Mudd SH, Irreverre F, Laster L. Sulfite oxidase deficiency in man: demonstration of the
966 enzymatic defect. Science. 1967;156(3782):1599-602. Epub 1967/06/23. doi:
967 10.1126/science.156.3782.1599. PubMed PMID: 6025118.
968 49. Dominy JE, Jr., Hirschberger LL, Coloso RM, Stipanuk MH. In vivo regulation of cysteine
969 dioxygenase via the ubiquitin-26S proteasome system. Adv Exp Med Biol. 2006;583:37-47. Epub
970 2006/12/13. doi: 10.1007/978-0-387-33504-9_4. PubMed PMID: 17153587.
971 50. Dominy JE, Jr., Hirschberger LL, Coloso RM, Stipanuk MH. Regulation of cysteine
972 dioxygenase degradation is mediated by intracellular cysteine levels and the ubiquitin-26 S
973 proteasome system in the living rat. Biochem J. 2006;394(Pt 1):267-73. Epub 2005/11/03. doi:
974 10.1042/bj20051510. PubMed PMID: 16262602; PubMed Central PMCID: PMCPMC1386025.
975 51. Stipanuk MH, Hirschberger LL, Londono MP, Cresenzi CL, Yu AF. The ubiquitin-
976 proteasome system is responsible for cysteine-responsive regulation of cysteine dioxygenase
977 concentration in liver. Am J Physiol Endocrinol Metab. 2004;286(3):E439-48. Epub 2003/12/03.
978 doi: 10.1152/ajpendo.00336.2003. PubMed PMID: 14644768.
979 52. Lee JI, Londono M, Hirschberger LL, Stipanuk MH. Regulation of cysteine dioxygenase
980 and gamma-glutamylcysteine synthetase is associated with hepatic cysteine level. J Nutr

981 Biochem. 2004;15(2):112-22. Epub 2004/02/20. doi: 10.1016/j.jnutbio.2003.10.005. PubMed
982 PMID: 14972351.
983 53. Kwon YH, Stipanuk MH. Cysteine regulates expression of cysteine dioxygenase and
984 gamma-glutamylcysteine synthetase in cultured rat hepatocytes. Am J Physiol Endocrinol Metab.
985 2001;280(5):E804-15. Epub 2001/04/05. doi: 10.1152/ajpendo.2001.280.5.E804. PubMed PMID:
986 11287364.
987 54. Baba T, Ara T, Hasegawa M, Takai Y, Okumura Y, Baba M, et al. Construction of
988 Escherichia coli K-12 in-frame, single-gene knockout mutants: the Keio collection. Mol Syst Biol.
989 2006;2:2006.0008. Epub 2006/06/02. doi: 10.1038/msb4100050. PubMed PMID: 16738554;
990 PubMed Central PMCID: PMCPMC1681482.
991 55. Mattingly BC, Buechner M. The FGD homologue EXC-5 regulates apical trafficking in C.
992 elegans tubules. Dev Biol. 2011;359(1):59-72. Epub 2011/09/06. doi:
993 10.1016/j.ydbio.2011.08.011. PubMed PMID: 21889936; PubMed Central PMCID:
994 PMCPMC3212395.
995 56. Lehrbach NJ, Ji F, Sadreyev R. Next-Generation Sequencing for Identification of EMS-
996 Induced Mutations in Caenorhabditis elegans. Curr Protoc Mol Biol. 2017;117:7.29.1-7..12. Epub
997 2017/01/07. doi: 10.1002/cpmb.27. PubMed PMID: 28060408; PubMed Central PMCID:
998 PMCPMC5303615.
999 57. Community G. The Galaxy platform for accessible, reproducible and collaborative
1000 biomedical analyses: 2022 update. Nucleic Acids Res. 2022;50(W1):W345-51. Epub 2022/04/22.
1001 doi: 10.1093/nar/gkac247. PubMed PMID: 35446428; PubMed Central PMCID:
1002 PMCPMC9252830.
1003 58. Bolger AM, Lohse M, Usadel B. Trimmomatic: a flexible trimmer for Illumina sequence
1004 data. Bioinformatics. 2014;30(15):2114-20. Epub 2014/04/04. doi: 10.1093/bioinformatics/btu170.
1005 PubMed PMID: 24695404; PubMed Central PMCID: PMCPMC4103590.
1006 59. Li H, Durbin R. Fast and accurate long-read alignment with Burrows-Wheeler transform.
1007 Bioinformatics. 2010;26(5):589-95. Epub 2010/01/19. doi: 10.1093/bioinformatics/btp698.
1008 PubMed PMID: 20080505; PubMed Central PMCID: PMCPMC2828108.
1009 60. Wilm A, Aw PP, Bertrand D, Yeo GH, Ong SH, Wong CH, et al. LoFreq: a sequence-quality
1010 aware, ultra-sensitive variant caller for uncovering cell-population heterogeneity from high-
1011 throughput sequencing datasets. Nucleic Acids Res. 2012;40(22):11189-201. Epub 2012/10/16.
1012 doi: 10.1093/nar/gks918. PubMed PMID: 23066108; PubMed Central PMCID:
1013 PMCPMC3526318.
1014 61. Cingolani P, Patel VM, Coon M, Nguyen T, Land SJ, Ruden DM, et al. Using Drosophila
1015 melanogaster as a Model for Genotoxic Chemical Mutational Studies with a New Program,
1016 SnpSift. Front Genet. 2012;3:35. Epub 2012/03/22. doi: 10.3389/fgene.2012.00035. PubMed
1017 PMID: 22435069; PubMed Central PMCID: PMCPMC3304048.
1018 62. Cingolani P, Platts A, Wang le L, Coon M, Nguyen T, Wang L, et al. A program for
1019 annotating and predicting the effects of single nucleotide polymorphisms, SnpEff: SNPs in the
1020 genome of Drosophila melanogaster strain w1118; iso-2; iso-3. Fly (Austin). 2012;6(2):80-92.
1021 Epub 2012/06/26. doi: 10.4161/fly.19695. PubMed PMID: 22728672; PubMed Central PMCID:
1022 PMCPMC3679285.
1023 63. Mello CC, Kramer JM, Stinchcomb D, Ambros V. Efficient gene transfer in C.elegans:
1024 extrachromosomal maintenance and integration of transforming sequences. Embo j.
1025 1991;10(12):3959-70. Epub 1991/12/01. doi: 10.1002/j.1460-2075.1991.tb04966.x. PubMed
1026 PMID: 1935914; PubMed Central PMCID: PMCPMC453137.
1027 64. Stiernagle T. Maintenance of C. elegans. WormBook. 2006:1-11. Epub 2007/12/01. doi:
1028 10.1895/wormbook.1.101.1. PubMed PMID: 18050451; PubMed Central PMCID:
1029 PMCPMC4781397.

1030 65. Schmittgen TD, Livak KJ. Analyzing real-time PCR data by the comparative C(T) method.
1031 Nat Protoc. 2008;3(6):1101-8. Epub 2008/06/13. doi: 10.1038/nprot.2008.73. PubMed PMID:
1032 18546601.
1033